Design and Optimization of a Self-powered Thermoelectric Car Seat Cooler

Daniel Benjamin Cooke

Thesis submitted to the faculty of the Virginia Polytechnic Institute and State University
in partial fulfillment of the requirements for the degree of

Master of Science
In
Mechanical Engineering

Zhiting Tian, Chair
Scott T. Huxtable, Co-Chair
Lei Zuo, Co-Chair

May 8, 2018
Blacksburg, Virginia

Keywords: Non-dimensional Equations, Solar Thermoelectric Generator, Thermoelectric Cooler

Design and Optimization of a Self-powered Thermoelectric Car Seat Cooler

Daniel Benjamin Cooke

Abstract

It is well known that the seats in a parked vehicle become very hot and uncomfortable on warm days. A new self-powered thermoelectric car seat cooler is presented to solve this problem. This study details the design and optimization of such a device. The design relates to the high level layout of the major components and their relation to each other in typical operation. Optimization is achieved through the use of the ideal thermoelectric equations to determine the best compromise between power generation and cooling performance. This design is novel in that the same thermoelectric device is utilized for both power generation and for cooling. The first step is to construct a conceptual layout of the self-powered seat cooler. Using the ideal thermoelectric equations, an analytical model of the system is developed. The model is validated against experimental data and shows good correlation. Through a non-dimensional approach, the geometric sizing of the various components is optimized. With the optimal design found, the performance is evaluated using both the ideal equations and though use of the simulation software ANSYS. The final design consists of a flat absorber plate embedded into the car seat with a thermoelectric attached to the back. A finned heat sink is used to cool the thermoelectric. The device is shown to generate enough power to provide a reasonable temperature drop in the seat.

Design and Optimization of a Self-powered Thermoelectric Car Seat Cooler

Daniel Benjamin Cooke

General Audience Abstract

It is well known that the seats in a parked vehicle become very hot and uncomfortable on warm days. A new self-powered thermoelectric car seat cooler is presented to solve this problem. The term thermoelectric refers to devices which convert thermal energy directly to electrical energy and can also convert electrical energy to thermal energy. This study details the design and optimization of such a device. Design relates to the layout and relationship of the major components. Optimization refers to the best use the given components to maximize power output and seat cooling. The final design consists of a flat absorber plate embedded into the car seat with a thermoelectric attached to the back. A finned heat sink is used to cool the thermoelectric. The device is shown to generate enough power to provide a reasonable temperature drop in the seat.

Acknowledgements

I would like to extend my thanks to Dr. Zhiting Tian for being my adviser throughout my Master's studies. She has been very helpful in my development professionally and in aiding me in reaching my academic goals. Additionally, she has provided me feedback and guidance throughout this project.

I would like to thank my committee members, Dr. Scott Huxtable and Dr. Lei Zuo, for agreeing to be on my committee and taking the time ask me questions and giving me additional advice.

Lastly, I would like to thank my mother, father, and my sister. I am grateful for their consistent support throughout my academic career. Without them I would not be where I am today.

Table of Contents

List of Figures

List of Tables

Nomenclature

A	Area of thermoelectric leg (mm^2)
A_{abs}	Area of absorber (m^2)
A_{fin}	Area of heat sink fin (m^2)
A_{TE}	Total area of thermoelectric device (m^2)
A_{total}	Total convective area of heat sink (m^2)
b_0	Height of heat sink fin (m)
COP	Coefficient of performance
El	Elenbaas number
g	Gravitational constant (m/s^2)
h	Convective coefficient (W/m^2K)
I	Current, (A)
k	Thermal conductivity (W/mK)
K	Total thermal conductivity (W/mK)
L	Length of thermoelectric leg (mm)
n	Number of thermoelectric leg pairs
n_{fin}	Number of heat sink fins
N_k	Dimensionless thermal conductance
N_I	Dimensionless current
N_{1c}	Dimensionless convectance of absorber plate
N_{2c}	Dimensionless convectance of heat sink
N_{1s}	Dimensionless radiation of absorber plate

N_{2s}	Dimensionless radiation of heat sink
N_{12rad}	Dimensionless radiation of ceramic plates
Nu	Nusselt number
q''	Solar irradiance (W/m^2)
$\dot{Q}_j$	Joule heating (W)
$\dot{Q}_t$	Thomson heating (W)
Ra	Rayleigh Number
R	Total electrical resistance (Ω)
R_r	Dimensionless load resistance
S	Length of heat sink (m)
t	Time (hrs)
t_0	Thickness of heat sink fin (m)
T	Temperature (K)
T_{max}	Maximum outdoor temperature ($°C$)
T_{min}	Minimum outdoor temperature ($°C$)
V	Voltage (V)
W_b	Width of heat sink (m)
z	Spacing of heat sink fins (m)
Z	Figure of merit ($1/K$)

Greek Letters

α	Seebeck coefficient, (V/K)

α_{abs}	Absorptivity of absorber plate
β	Volumetric thermal expansion of air $(1/K)$
ϵ	Emissivity
η	Efficiency
Π	Peltier coefficient (W/A)
ρ	Electrical resistivity $(\Omega\, m)$
σ	Stefan Boltzmann constant (W/m^2K^2)
τ	Thomson coefficient $(W/A°C)$
τ_{glass}	Transmittance of windshield glass
υ	Kinematic viscosity of air (m^2/s)
ω	Thermal diffusivity of air (m^2/s)

Subscripts/superscripts

abs	Absorber
n	N-leg
p	P-leg
sur	Surroundings
TE	Thermoelectric
1	Absorber
2	Heat sink
$1c$	Convection of absorber plate
$2c$	Convection of heat sink
$1rad$	Radiation of absorber plate

$2rad$	Radiation of heat sink
$12rad$	Radiation of TE ceramic plates
$*$	Dimensionless property

Chapter 1: Introduction and Background

1.1) Introduction

The thermoelectric effect is the combination of three phenomena: the Seebeck effect, the Peltier effect, and the Thomson effect. The Seebeck effect occurs when a temperature difference exists between the junctions of two dissimilar conductors and results in a potential difference [1]. The reverse process is called the Peltier effect, in which a potential difference applied across two conductors results in a temperature difference [2]. The Thomson effect states that if a conductor which has a current passing through it also experiences a temperature difference, then heat will be either absorbed or emitted by the conductor, depending on the thermal gradient and the direction of flow of current [3]. Thermoelectric devices utilize these effects to operate. Most thermoelectrics used today fall into two main categories: thermoelectric generators (TEGs) and thermoelectric coolers (TECs).

TEGs are used to convert thermal energy in the form of a temperature difference into electrical energy. Notable devices which have utilized this technology include the Lincoln Experimental Satellites and the Voyager space probes [4]. Each of these spacecraft were powered by TEGs which used heat generated by nuclear fission. More recently, TEGs have been used to produce small amounts of energy from waste heat sources. Consumer products, such as camp stoves which produce electrical power, have made thermoelectrics mainstream [5]. Additionally, many researchers have built and tested solar powered TEGs [6]. Future applications of thermoelectrics are broad. Current proposals suggest that they could be used to harvest energy from the human body to power health monitoring systems [7]. TECs have also found uses in many products. These devices utilize electrical energy to produce thermal gradient, in effect acting as a

heat pump. Several manufacturers currently provide portable coolers and climate controlled car seats which utilize TECs [8,9]. They have also been proposed as a means to cool electronic components [10].

As seen, thermoelectric devices have many diverse uses. The main advantage of TECs and TEGs is that they have no moving parts. For this reason, they are reliable, long lasting, and can operate quietly. However, these devices do possess downsides. TEGs suffer from low conversion efficiencies. Additionally, the materials currently used to manufacture thermoelectrics are costly. Despite these shortcomings, thermoelectrics are a versatile technology.

1.2) Problem Overview

It is commonly known that the interior of automobiles become very hot in the summertime. Air temperatures inside a parked car exposed to direct sunlight can reach in excess of 60°C on a summer day [11]. Surface temperatures can be in excess of 90°C [12]. When an occupant enters the vehicle in these conditions it is very uncomfortable. Both the cabin air and the car seat are hot. Several devices have been developed to provide cooling to the occupant, with varied success. The most common solution is the use of the vehicle's air conditioning system. While this method does cool the interior, it takes time to reach a comfortable temperature. Even if cold air is supplied during this cool down period, the car seat is still very hot.

In looking to solve this problem, it is important to note that there are two phenomenon occurring. The first is that for the majority of the day, most vehicles are inundated with solar energy. The second is that because of this solar energy, the car seat is very hot and uncomfortable. In studying this problem, a solution to the second

problem is found in the first. A possible solution is to capture and store solar energy over the course of the day. Then, when the occupant returns to the vehicle this energy is used to cool the car seat. In searching for a means to accomplish this, thermoelectrics are introduced as a viable technology since these devices can both generate electrical energy and also provide thermal cooling. The proposed operation of such a device is as follows. First, during the day a thermoelectric is used to generate electrical energy from a temperature difference created by solar irradiance. This energy is stored in a battery for later use. When the occupant of the vehicle returns and cooling is desired, a thermoelectric embedded in the seat will utilize the stored electrical energy to cool the car seat.

The use of thermoelectrics in car seat cooling is not new. As previously mentioned, several manufactures sell commercial thermoelectric car seat coolers. The first application of thermoelectrics to car seat comfort was by Malvicino et al. in 2001 [13]. Using a thermoelectric device to cool the occupant of the vehicle has several advantages over other cooling solutions. For example, one seat cooling solution is to force air through the seat. While this does provide convective cooling, the air used is still at the ambient temperature of the vehicle. A thermoelectric cooler is more effective because it provides active heat removal from the seat by either first cooling the air supplied to the occupant or by directly cooling the seat through conduction. The most common device used to cool the seat is the vehicle's air conditioning system. However, this cools indirectly by first reducing the temperature of the interior air. The air then cools the seat and occupant. By using a thermoelectric seat cooler, cooling is provided directly to the seat.

Furthermore, the self-powered thermoelectric car seat cooler has power advantages over other forms of vehicle cooling. The standard air conditioning system has been shown to increase fuel consumption by 28% for light duty vehicles [14]. This increase in load is not insignificant. Other proposed thermoelectric seat cooler designs will also increase the load on the vehicle's engine and/or electrical system. The self-powered thermoelectric seat cooler does not experience this problem because this device is self-powered. It can operate while the car is parked and the engine is not running.

The design is made further unique in that same thermoelectric device is used for both power generation and for cooling. To our knowledge, this paper is the only study to research the operation of such a device. This design choice not only expands the field of study of thermoelectrics, but it also improves the design of the seat cooler. By embedding the cooler/generator directly into the seat, the device does not impact the aesthetics of the vehicle interior. This allows it to be easily implemented into current and future vehicle designs.

1.3) Thermoelectric Governing Effects

As previously mentioned, the thermoelectric effect is described by the Seebeck, the Peltier, and the Thomson effects. This section will briefly cover these phenomenon in detail.

The Seebeck effect is the direct conversion of thermal energy into electrical energy. This effect is what allows thermocouples to measure temperature. In Figure 1. 1, two conductors are joined electrically in series and thermally in parallel. One material is a p-type and the other is a n-type. The difference in these materials are the impurities which are introduced, which is achieved through doping. The naming convention of the

materials comes from the terminology used in doping, where p represent the electron hole concentration, and n represents the free electron concentration.

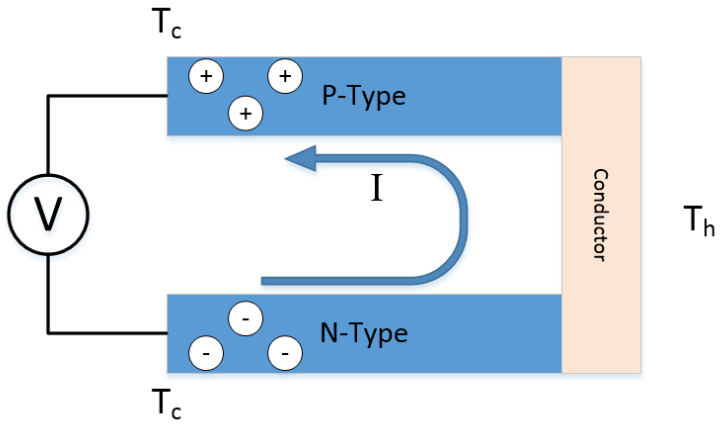

Figure 1. 1 Seebeck effect

If a temperature difference is applied across the two legs, given as T_h for the hot side temperature and T_c for the cold side temperature, then thermal energy added at the hot end of the conductor frees electrons causing them to diffuse to cold end [15]. This diffusion creates a voltage difference in the thermoelectric material. This voltage is calculated by

$$V = \alpha \Delta T, \tag{1. 1}$$

where α is the Seebeck coefficient and ΔT is the temperature difference across the materials.

The Peltier effect states that when a current is passed through the intersection of two conductors then heat is released on one side and absorbed on the other. The reason for this is similar to the Seebeck effect. The applied current causes electrons to flow through the thermoelectric. In doing so the electrons carry thermal energy from one side to the other. The heat flow from the intersection is governed by:

$$Q_{Peltier} = \Pi I = \alpha T I, \tag{1. 2}$$

where Π is the Peltier coefficient and I is the current. This is seen in Figure 1. 2 below.

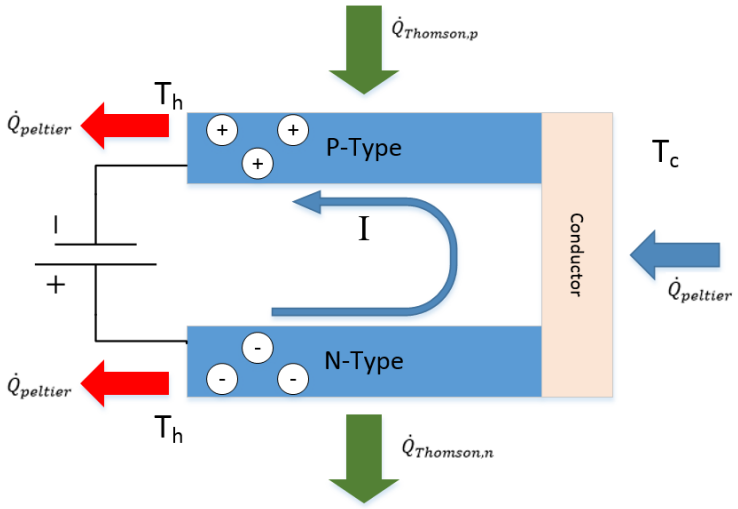

Figure 1. 2 Peltier and Thomson effect

The Thomson effect occurs when there is temperature gradient across a conductor accompanied by a current. Heat can either be released or absorbed depending on the flow of current and the temperature gradient. The amount of heat absorbed or released is

$$Q_{Thomson} = \tau I \Delta T, \tag{1. 3}$$

where τ is the Thomson coefficient and is given as

$$\tau = T \frac{d\alpha}{dT}. \tag{1. 4}$$

The Thomson effect is the only thermoelectric effect which can be experienced by a single conductor. The Seebeck and Peltier effects require that two conductors are connected at a junction.

The final concept introduced in this section is the figure of merit. This is an important term used to describe thermoelectric materials. It is denoted by

$$Z = \frac{\alpha^2}{\rho k} \tag{1. 5}$$

where ρ is the electrical resistivity of the material and k is the thermal conductivity. The units of Z are $1/K$. The higher the figure of merit, the better suited a material is for thermoelectric applications. This term relates the power production capabilities of the material to its electrical and thermal properties. The ideal thermoelectric material would have a large Seebeck coefficient and low thermal conductivity and electrical resistance. A material such as this would allow current to flow freely through it while maintaining a large thermal gradient. Typically, the figure of merit is multiplied by the absolute temperature to obtain the non-dimensional figure of merit or ZT value. Currently, ZT values are about 1 for most thermoelectric materials [15].

Chapter 2: Project objective and literature review

2.1) Project Objectives

This study seeks to design a self-powered thermoelectric car seat cooler. In setting out to plan this device, many aspects of thermoelectric design are considered. Assumptions and justifications used in the design and modeling of the final device are listed. The following chapters link both analytical and experimental data to provide the most realistic results. This study also displays the proof of concept of a theoretical thermoelectric device.

Another aspect of this study is that it acts as a roadmap for others seeking to design thermoelectric devices. The details given are thorough in that both thermoelectric cooling and thermoelectric power generation are covered. Using the given methodology, designers wishing to utilize thermoelectrics can follow the steps outlined to choose the optimal parameters of the device and to model the predicted performance.

The optimization used in this study is modified from a method developed by Lee [16]. This technique is very useful in the design of thermoelectrics. Without it, choosing the ideal parameters for a thermoelectric device would require the variation of many different properties. Additionally, this method states that for a given loading condition, an optimal design of the thermoelectric does exist.

Focusing on this specific study, the problem posed is to design a thermoelectric car seat cooler which is powered by a solar thermoelectric generator. This design is novel in that the same thermoelectric device will be used for both power generation and for cooling the seat. Therefore, the thermoelectric design will be optimized under two conditions. The first condition is the solar heating of the device. The second is the

design for optimal cooling. To provide a proof of concept for this novel design, the goals of this study are as follows:

1) Provide a high level design of the self-power thermoelectric car seat cooler by listing the major components and showing their relationship to each other.
2) Develop and validate a one-dimensional analytical model using the ideal thermoelectric equations to simulate the design outlined in part 1.
3) Optimize the geometry and operation of the self-powered seat cooler through an iterative non-dimensional method.
4) Simulate the optimized device performance under typical operating conditions and compare the results to an ANSYS simulations.

Through this methodology, the performance of the proposed device is determined. Ultimately, this shows whether the design is feasible.

2.2) Literature Review

In preparing for this study, it is important to consider research in the field of thermoelectrics. This section is broken down into three categories: solar powered thermoelectric generators, thermoelectric seat cooling, and thermoelectric use in combined power generation and cooling.

Several studies have focused on the use of solar thermoelectric generators (STEGs). These devices normally consist of a solar collection device, the thermoelectric, and some form of heat dissipation. Early experiments by Goldsmid et al. studied STEGs using Bismuth Telluride [17]. The main goal was to see how well a thermoelectric generator can convert solar energy into electrical energy. In the study, two designs were proposed and tested. The first used a flat plate aluminum collector with two glass plates

to prevent heat from escaping. The second design was a semi-parabolic stationary solar concentrator which focused light onto the TEG. For the flat plate collector, a peak hot side temperature of $90°C$ was achieve with total temperature difference of $45°C$. This resulted in a max power output of about 0.75 W. While the flat plate was able to produce power, it was only able to achieve an overall system efficiency of 1%. The solar concentrator was able to reach higher temperatures of about $120°C$. Despite reaching a larger hot side temperature than the flat plate, the stationary solar concentrator only achieved an overall efficiency of 0.5%. This was mainly due to design limitations. Goldsmid et al. predicted that with improved collector efficiency, the total efficiency could rise to 3%.

A similar study was performed by Amatya et al. who also used a solar concentrator to direct sunlight toward a Bi_2Te_3 thermoelectric module [18]. The cold side was cooled using a natural convection pin fin heat sink. The thermoelectric used in this study was a TG12-4 from Marlow Inc. Using the concentrator and heat sink, the TEG was able to produce 1.8 W of power at a system efficiency of around 3%. The main conclusion was that well designed STEGs are an attractive method for micro power applications.

Several studies have looked at the use of thermoelectric coolers in automobiles. M. Vinoth and D. Prema designed an automated safety cooling system for car seats [19]. This system is designed to protect small children in the case of being left in a hot vehicle by providing direct convection cooling to the child. In this design, cold air is supplied to the seat through use of a thermoelectric heat exchanger. The final device was able to maintain the ambient air temperature around the child's car seat at $32°C$ to $25.8°C$. This

temperature was obtained within three minutes of the thermoelectric cooler being activated.

Elarusi el al. optimized the design of a thermoelectric car seat cooling/heating system [20]. This design delivered conditioned air to the occupant by using a thermoelectric with heat sinks attached on both the hot and cold sides. Interior car air was then either cooled or heated and delivered to the occupant through a perforated seat. A model of the system was developed and compared to experimental data obtained by Feher [21]. Good agreement was found between the two. This model was then used to optimize the TEC and simulate its performance. The optimization method was non-dimensionalized according to the thermal convection conductance of the hot air stream. For the cooling operation, a temperature difference of $11°C$ was reported for an ambient air temperature of $27°C$. The cooling power was predicted to be 18.61 W and the power consumption was 40.95 W [20].

Su et al. also modeled and tested a thermoelectric car seat cooler [22]. Like Elarusi et al., this design also utilized finned heat sinks on both the hot and cold side to supply conditioned air. In this study, CFD modeling was used to determine the number of thermoelectric modules needed. Simulation results showed that the setup should use two thermoelectrics to convectively cool the air. The experimental setup supplied cooled air through the back of the seat to cool the occupant. At an ambient temperature of $32.7°C$, the device was able to reduce the passenger's back temperature from $33.4°C$ to $28.2°C$. The temperature drop was achieved in 60 seconds with the TEC operating at 4 amps.

Research has also been focused on the use of TEGs to power a TEC. One such study was performed by Khattab and Shenawy who used several STEGs to power a TEC [23]. Using Bi_2Te_3 thermoelectrics, they constructed both a STEG and a TEC. The STEG used a reflector to focus solar light onto an absorber plate. The TEC cold side was used to cool a mass of water, while the hot side was cooled by a heat sink. The study looked at the performance of such a device throughout the year as the ambient temperature and solar input varied. It was concluded that multiple TEGs would be required to power the TEC.

A similar study is performed by Chen et al. who simulated the performance of a single TEC connected to a single TEG [24]. The simulation looked at how the boundary conditions and leg lengths affected the performance. ANSYS was used to model the performance of the device at several different conditions. The model consisted of two thermoelectric leg pairs, one pair for the cooler and the other for the generator. It was noted that the geometry of the legs plays a significant role in the performance of the whole system. The range of cooling was found to be about $10\ mW - 100\ mW$. As in the previous study by Khattab and Shenawy, it was concluded that a feasible design would incorporate multiple TEGs to power the TEC.

Du et al. investigated using TEGs which collected power from automobile exhaust to power a car seat TEC [25]. The main point of this study was to verify that such a setup was possible. Through experiments, it was shown that the TEG was able to produce over 250 watts of power depending on the working conditions of the engine. The temperature controlled seat was similar in design to the other seat coolers presented. It consisted of a blower, 4 fans and a TEC. The total power consumption of the entire

system was 73.2 W. Therefore, the exhaust system provided enough power to effectively operate the seat. Although enough power is supplied by the TEG, a battery is still used to compensate for any variance in voltage of the generator. In testing, the TEC was able to reduce the seat temperature from $36.61°C$ to $31.27°C$ at ambient cabin air temperature of $42.33°C$. The device was able to reach steady state cooling in under 2 minutes.

Although the mentioned studies produced functional devices, they neglect a few key issues. The first critique applies to both TEGs and TECs. Most of the designs, with a few exceptions, do not use optimization techniques to choose the proper thermoelectric geometry or operating conditions for their device. While the devices are still functional, their performance would be greatly improved if the proper characteristics were chosen based on the predicted boundary conditions. Additionally, most designs of thermoelectric car seat coolers give little consideration to the device power requirements and whether or not the vehicle is capable of supplying this power. Lastly, the designs presented are not shown to be tested at varying operating conditions. Without a comparison to other conditions, it is difficult to determine a baseline which the performance can be compared to.

These concerns are addressed in this paper. The design of the thermoelectric device is chosen through a non-dimensional optimization routine. Power considerations for the final design are eliminated due to the fact that the thermoelectric seat cooler is self-powered. Finally, the design is tested under different operating conditions and a baseline case is shown to draw comparison to.

Chapter 3: Device Design and Modeling

This chapter will cover all the necessary concepts needed for the design. This includes all the tools and validations used to design the final device. It begins with the derivation of the equations used throughout the analysis. This includes the ideal thermoelectric equations, a one-dimensional model of the device, and the non-dimensional form of the model. The high level design is given along with justifications for the specific layout. Finally, several noteworthy studies are introduced which aid in validating the analytical model.

3.1) Thermoelectric Ideal Equations

Consider a thermoelectric device shown in Figure 3. 1 below. It consists of two legs, p and n, made of different thermoelectric materials. The legs are thermally in parallel and electrically in series. A temperature gradient exists between the top and bottom of the legs. The length and cross sectional area of both legs are identical.

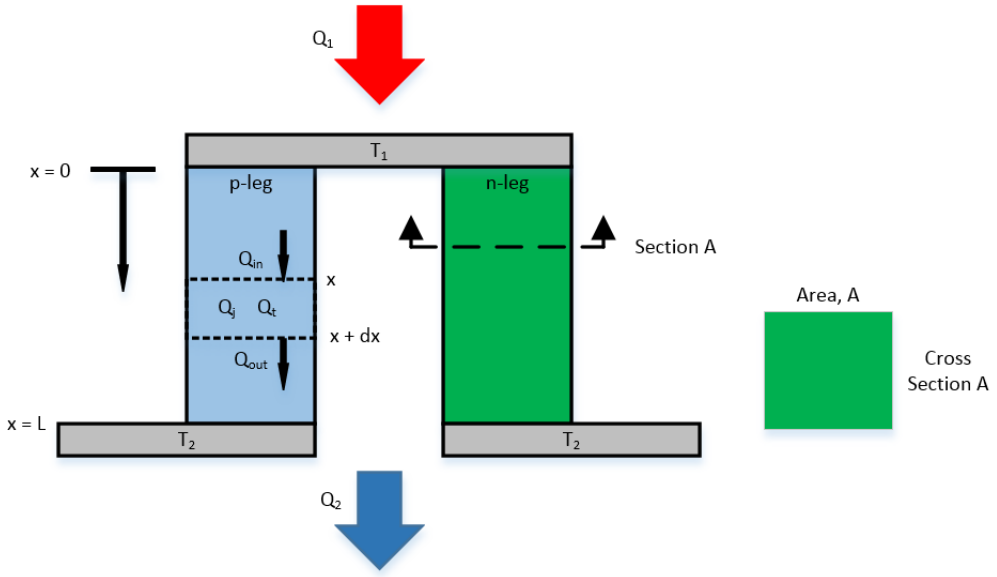

Figure 3. 1 Control volume for a typical thermoelectric device.

The heat flow is described using the Thomson relationship and Onsager's principle. This relationship is given as [26]

$$\dot{Q} = \alpha T I - k\frac{dT}{dx} \tag{3. 1}$$

where k is the thermal conductivity of the thermoelectric material. This equation relates the heat flow to the Peltier cooling and thermal conduction. A differential control volume is drawn around a section of the p-leg. Although the following analysis is performed for the p-leg, it also applies to the n-leg. Assuming one-dimensional steady-state conditions, the conservation of energy gives

$$\dot{Q}_{in} - \dot{Q}_{out} + \dot{Q}_j + \dot{Q}_t = 0 \tag{3. 2}$$

where Q_{in} is the Fourier heat conduction into the control volume, Q_{out} is the Fourier heat conduction out of the control volume, Q_j is the Joule heating generated inside the control volume, and Q_t is the Thomson heat due to the Thomson effect. This can be written as

$$\dot{Q}(x) - \dot{Q}(x + dx) + \dot{Q}_j + \dot{Q}_t = 0. \tag{3. 3}$$

Applying a first order Taylor expansion to the second term in Equation (3. 3) and expanding the other terms results in

$$\dot{Q}(x) - \left(\dot{Q}(x) + \frac{d\dot{Q}(x)}{dx}dx\right) + \frac{I^2\rho_p}{A_p}dx - \tau I dT = 0 \tag{3. 4}$$

The equation can be further expanded by using the Fourier's Law of Conduction given as

$$\dot{Q}(x) = -k_p A_p \frac{dT}{dx}. \tag{3. 5}$$

Equation (3. 4) then becomes

$$\frac{d}{dx}\left(k_p A_p \frac{dT}{dx}\right)dx + \frac{I^2\rho_p}{A_p}dx - \tau_p I dT = 0. \tag{3. 6}$$

The thermoelectric properties in the differential equation, k_p, ρ_p, and τ_p, all vary with temperature and the temperature varies with x along the leg. This makes the equation unsolvable analytically. However, if it is assumed that the thermoelectric properties are constant, Equation (3. 6) reduces to

$$\frac{d}{dx}\left(k_p A_p \frac{dT}{dx}\right)dx + \frac{I^2 \rho_p}{A_p}dx = 0. \tag{3. 7}$$

The boundary conditions are $T_{x=0} = T_1$ and $T_{x=L} = T_2$. By integrating Equation (3. 7) and applying the boundary conditions:

$$\left.\frac{dT}{dx}\right|_{x=0} = \frac{(T_2 - T_1)}{L_p} + I^2 \frac{\rho_p L_p}{2k_p A_p^2} \tag{3. 8}$$

$$\left.\frac{dT}{dx}\right|_{x=L} = \frac{(T_2 - T_1)}{L_p} - I^2 \frac{\rho_p L_p}{2k_p A_p^2}. \tag{3. 9}$$

Combining Equations (3. 8), (3. 9), and (3. 1), the heat flow at the top of the p-leg is given by

$$\dot{Q}_p(x = 0) = \alpha_p T_1 I - \frac{I^2 \rho_p L_p}{2A_p} + \frac{A_p\, k_p}{L_p}(T_1 - T_2) \tag{3. 10}$$

and the bottom of the leg given by

$$\dot{Q}_p(x = L) = \alpha_p T_2 I + \frac{I^2 \rho_p L_p}{2A_p} + \frac{A_p k_p}{L_p}(T_1 - T_2). \tag{3. 11}$$

Likewise, it can be shown that the heat flow for the n-leg is given by

$$\dot{Q}_n(x = 0) = -\alpha_n T_1 I - \frac{I^2 \rho_n L_n}{2A_n} + \frac{A_n k_n}{L_n}(T_1 - T_2) \tag{3. 12}$$

and

$$\dot{Q}_n(x = L) = -\alpha_n T_2 I + \frac{I^2 \rho_n L}{2A_n} + \frac{A_n k_n}{L_n}(T_1 - T_2). \tag{3. 13}$$

Summing the heat flow at $x = 0$ gives the heat flow into the top of the thermoelectric device. If the cross sectional areas and lengths of the legs are the same, this is expressed as

$$\dot{Q}_1 = n\left[(\alpha_p - \alpha_n)T_1 I - \frac{1}{2}I^2\left(\frac{\rho_p L}{A} + \frac{\rho_n L}{A}\right) + \left(\frac{k_p A}{L} + \frac{k_n A}{L}\right)(T_1 - T_2)\right] \quad (3.\ 14)$$

where n is the number of leg pairs in the thermoelectric device. Likewise at $x = L$

$$\dot{Q}_2 = n\left[(\alpha_p - \alpha_n)T_2 I + \frac{1}{2}I^2\left(\frac{\rho_p L}{A} + \frac{\rho_n L}{A}\right) + \left(\frac{k_p A}{L} + \frac{k_n A}{L}\right)(T_1 - T_2)\right]. \quad (3.\ 15)$$

Equations (3. 14) and (3. 15) can be simplified to

$$\dot{Q}_1 = n\left[\alpha T_1 I - \frac{1}{2}I^2 R + K(T_1 - T_2)\right] \quad (3.\ 16)$$

$$\dot{Q}_2 = n\left[\alpha T_2 I + \frac{1}{2}I^2 R + K(T_1 - T_2)\right] \quad (3.\ 17)$$

where

$$\alpha = \alpha_p - \alpha_n \quad (3.\ 18)$$

is the total Seebeck coefficient,

$$R = \frac{\rho_p L}{A} + \frac{\rho_n L}{A} \quad (3.\ 19)$$

is the total electrical resistance, and

$$K = \frac{k_p A}{L} + \frac{k_n A}{L} \quad (3.\ 20)$$

is the total thermal conductivity.

These are the ideal equations for a typical thermoelectric device. They are derived with the assumption that the material properties are constant throughout the length of the leg.

3.2) Validity of the Ideal Equations

The previous section derived the thermoelectric ideal equations assuming that the material properties are independent of temperature. However, these properties do change. Figure 3. 2 displays the temperature variance of the Seebeck coefficient, electrical resistivity, and thermal conductivity for nanocomposite Bi_2Te_3.

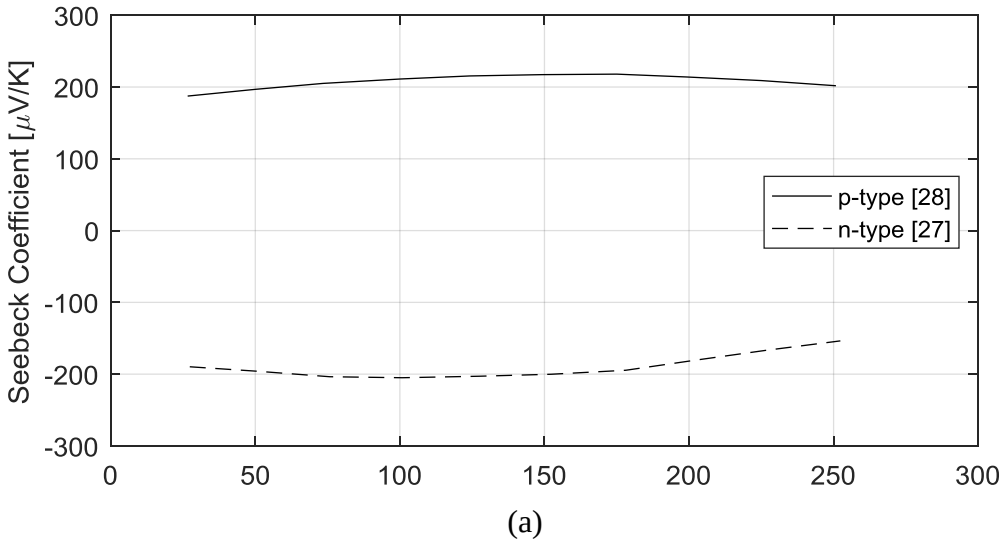

(a)

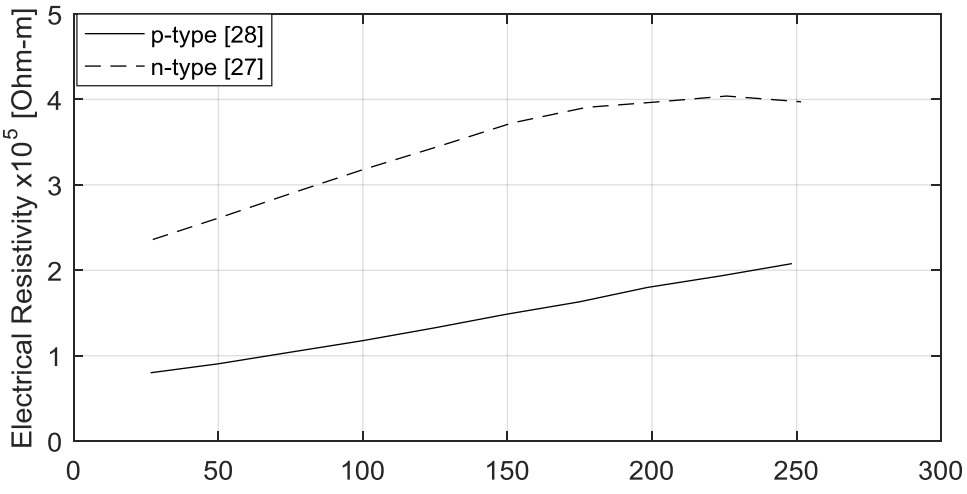

(b)

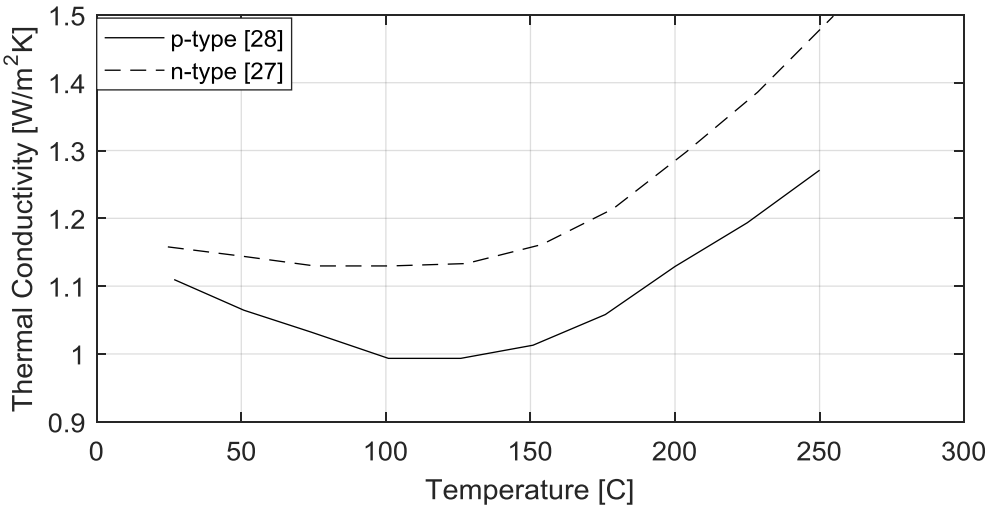

(c)

Figure 3. 2 Variance of (a) Seebeck coefficient, (b) electrical resistivity, and (c) thermal conductivity for p and n-type nanocomposite Bi_2T_3 [27,28].

A study by Kanimba et al. researched the accuracy of assuming constant material properties for thermoelectric generators by developing a one dimensional model which accounts for not only the temperature dependence of material properties, but also the Joule heating in the copper strips and heat losses through radiation and convection [29]. By modeling Lead Telluride (PbTe) at a temperature gradient of 570 K, it was shown that the efficiency and power of the ideal equation were reduced by 10% and 30% respectively. However, the material used in the current study is Bi_2Te_3 with possible temperature gradients ranging from 50 to 100 K. The model developed by Kanimba et al. is used to determine if the chosen material and operating conditions warrant the use of a detailed model. The material properties used are the same as shown in Figure 3. 2. Shown in Figure 3. 3 and Figure 3. 4 are the voltage and power output of Bi_2Te_3 over a range of currents. The results are for a single leg pair with an area of 1 mm^2 and a leg length of 1.2 mm. The cold side of the thermoelectric is held at 300K both cases. For voltage, the maximum error is 2.8% and for power the error is 2.9%.

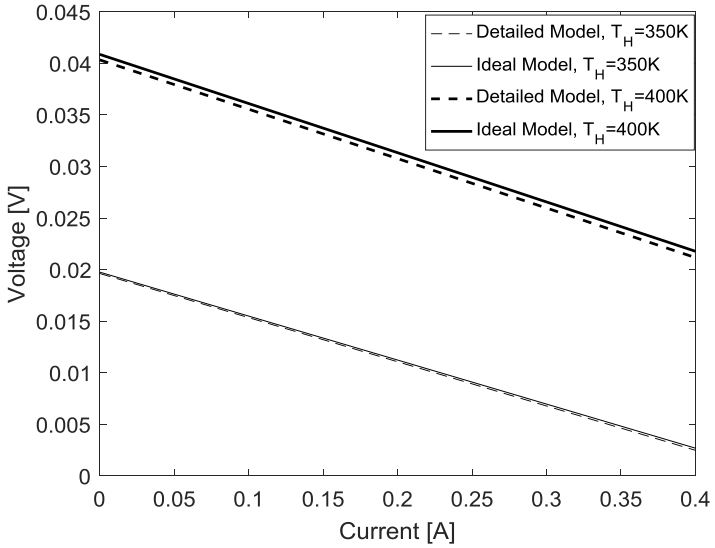

Figure 3. 3 Voltage comparison of ideal equations to detailed equations.

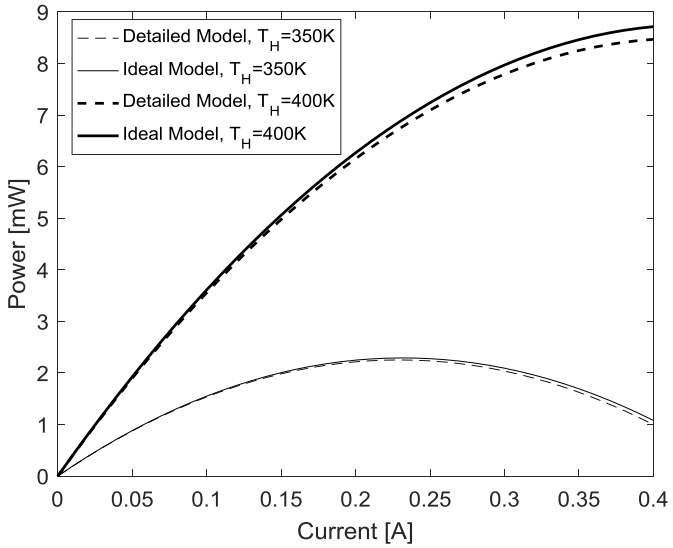

Figure 3. 4 Power comparison of the ideal equations to the detailed equations.

The use of the ideal equations are also valid when studying thermoelectric cooling effects. This is supported by Lee who looked to validate the use of the ideal equations for a thermoelectric cooler [30]. In this study the ideal equations were compared to the exact solution. The ideal solution assumed constant thermoelectric properties at the average

temperature of the hot and cold sides of the thermoelectric. The exact solution only accounted for the change of the Seebeck coefficient, and did not account for changes in either the thermal conductivity or the electrical resistivity. It was found that at low current and low temperature differences, the two equations show good agreement. As long as the material properties are taken at the average temperature of the hot and cold sides, then the ideal equations are satisfactory for analysis. However, as the current and temperature difference rise, the two solutions begin to diverge. This is shown in Figure 3. 5 and Figure 3. 6. In these plots, the exact solution is found using the thermal-electrical analysis tools in ANSYS. The results shown are for a thermoelectric with a leg length of 1.25 mm, a leg area of 1 mm^2, and 127 leg pairs. Looking at the curves in Figure 3. 5, the error between the last ANSYS data point and the ideal curve is about 8%. The curves seem to further diverge at higher currents. Therefore, as long as the thermoelectric cooler is operated at a low current and a low temperature difference, the ideal equations can accurately model performance.

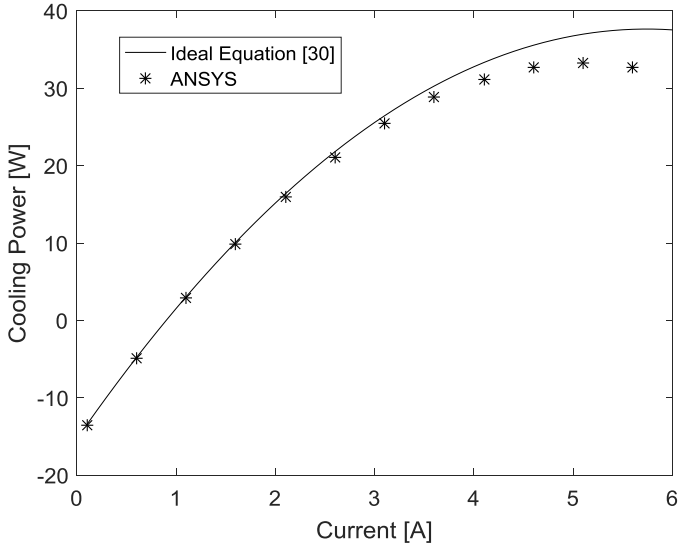

Figure 3. 5 Comparison of the ideal equations to the ANSYS solution where T_1 = 370 K and T_2=420 K

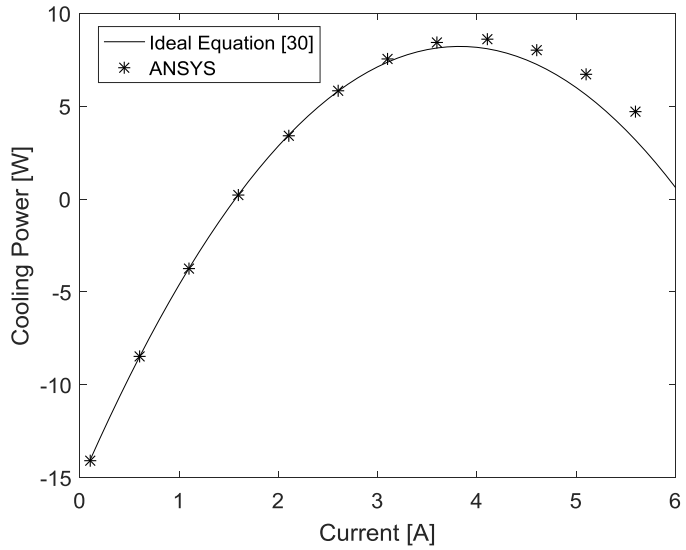

Figure 3. 6 Comparison of the ideal equations to the ANSYS solution where T_1=248 K and T_2=298 K.

From the two studies above, it is shown that the ideal equations derived in Section 3.1) are valid for modeling both power generation and cooling in thermoelectric devices.

3.3) Design of the self-powered car seat cooler

The design of the self-powered seat cooler is based on the conditions of the car interior. During a typical summer day, the interior of the car is heated to temperatures well above those of the outside of the car. This is due to solar energy that falls on the various interior surfaces, which include the steering wheel, dashboard, and car seats. This solar energy is absorbed and in response these surfaces heat up. In turn the surfaces convectively heat the air inside the car.

The intended operation of the self-powered thermoelectric seat cooler is as follows. Over the course of a day, the TEG is heated by the solar rays which fall upon it. This creates a temperature difference between the side of the thermoelectric exposed to the sun and the opposite side which is only exposed to the ambient air of the car. This

temperature difference is converted to electrical energy. When seat cooling is desired, the TEC uses the collected electrical energy to create a temperature difference between the seat and the interior temperature. To facilitate the heat removal during power generation and seat cooling, a finned heat sink is attached to the backside of the thermoelectric. To keep power needs minimal, natural convection is used to cool the heat sink. The design is initially thought of as two separate devices: a STEG and a TEC. However, these two functions can be combined into a single device. A thermoelectric can perform both operations of power generation and cooling. For this to work, the device needs to receive ample solar energy during the day, while also being close enough to the seat to provide cooling. Therefore the ideal setup is to embed the thermoelectric device into the seat. As stated previously, the seat receives ample solar energy. Additionally, by residing in the seat, the device can provide conductive cooling to the occupant. A high level conceptual drawing of the device is shown below in Figure 3. 7.

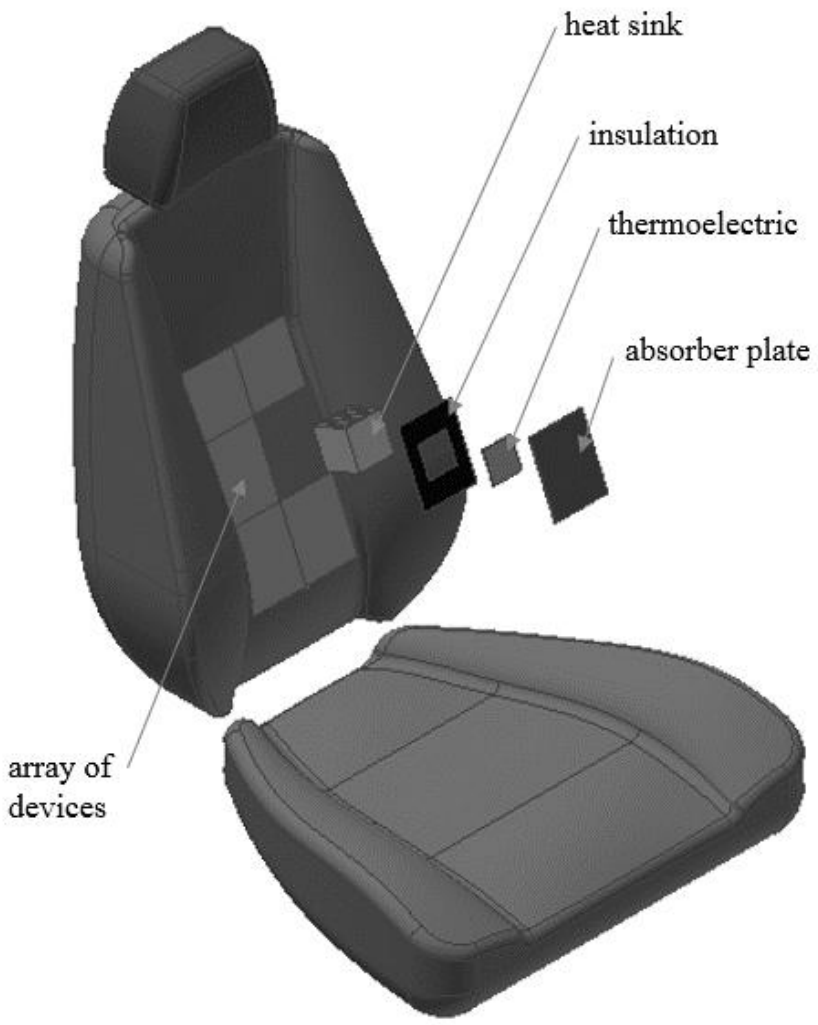

Figure 3. 7 Exploded view of proposed design.

The design consists of an embedded array of devices in the car seat. An absorber plate is used collect solar irradiance and heat the top surface of the thermoelectric. Covering the back of the absorber plate is insulation which prevents heat loss through the back side of the plate to radiation and convection. A heat sink is used to cool the thermoelectric and is open the back side of the seat. This orientation protects the heat sink from solar irradiance, while allowing it to dissipate heat to the interior cabin air. During cooling

operation, heat is pumped from the absorber plate, through the thermoelectric, and dissipated by the heat sink.

3.4) One-Dimensional Analytical Model

With a given design, the governing equations are determined by creating a control volume and performing an energy balance. Figure 3. 8 below depicts the flow of energy in the system.

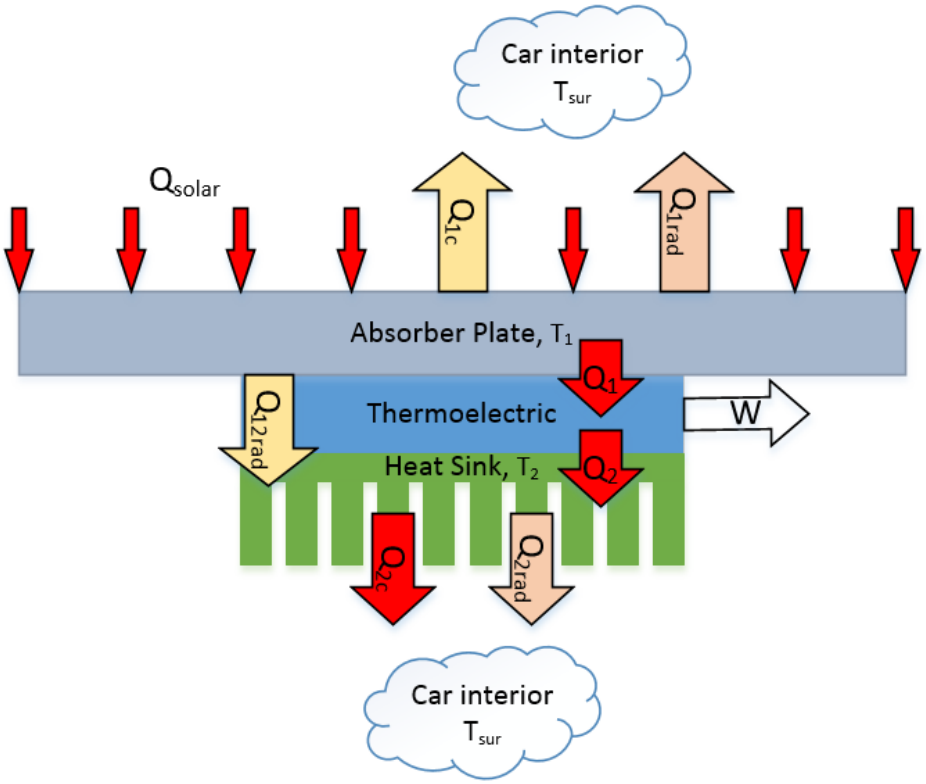

Figure 3. 8 Energy balance of self-powered thermoelectric seat cooler.

Solar irradiance, Q_{solar}, is absorbed by the top plate. The plate loses heat through convection, Q_{1c}, and radiation, Q_{1rad}, to the car interior. Energy which is not lost to the environment passes through the thermoelectric, Q_1, where a partial amount is converted to electrical energy, W, and the rest leaves the opposite side, Q_2, through the heat sink. Some energy is directly sent from the top plate to the bottom through radiation, Q_{12rad}.

The heat sink loses energy through radiation, Q_{2rad}, and convection, Q_{2c}, to the car interior. Performing an energy balance on the absorber, it is found that

$$\dot{Q}_1 = \dot{Q}_{solar} - \dot{Q}_{1c} - \dot{Q}_{12rad} - \dot{Q}_{1rad}. \tag{3. 21}$$

An energy balance on the thermoelectric reveals

$$\dot{W} = \dot{Q}_1 - \dot{Q}_2. \tag{3. 22}$$

The energy balance on the heat sink gives

$$\dot{Q}_2 = \dot{Q}_{12rad} - \dot{Q}_{2c} - \dot{Q}_{2rad}. \tag{3. 23}$$

Expanding Equation (3. 21), it is shown that

$$\begin{aligned} \dot{Q}_1 = \alpha_{abs}\tau_{glass}A_{abs}q_s'' - h_1A_{abs}(T_1 - T_{sur}) \\ - (A_{TE} - 2nA)\epsilon_{12}\sigma(T_1^4 - T_2^4) \\ - A_{abs}\epsilon_{1rad}\sigma(T_1^4 - T_{sur}^4), \end{aligned} \tag{3. 24}$$

where α_{abs} is the absorptivity of the conductive plate, τ is the transmittance of the windshield glass, A_{abs} is the area of the absorber plate, and q_s'' is the solar irradiance. The second term in Equation (3. 24) is the convective heat loss where h_{abs} is the convective coefficient of the absorber plate, T_1 is the temperature of the conductive plate and the top side of the thermoelectric, and T_{sur} is the temperature of the ambient air. A_{TEG} is the total area of the thermoelectric ceramic plate, n is the number of thermoelectric leg pairs, A_e is the cross sectional area of a single leg, ϵ_{12} is the emissivity between the ceramic plates of the thermoelectric, σ is the Stefan-Boltzmann constant, and T_2 is the temperature of the heat sink. In the last term, ϵ_{1s} is the emissivity between the absorber plate and the surroundings. Expanding Equation (3. 23)

$$\begin{aligned} \dot{Q}_2 = (A_{TE} - 2nA)\epsilon_{12rad}\sigma(T_1^4 - T_2^4) - h_2A_{2c}(T_2 - T_{sur}) \\ - A_{2rad}\epsilon_{2rad}\sigma(T_2^4 - T_{sur}^4), \end{aligned} \tag{3. 25}$$

where h_2 is the average convective heat transfer coefficient of the heat sink, A_{csink} is the convective area of the heat sink, and A_{rsink} is the radiative area of the heat sink.

This concludes the derivation of the thermoelectric equations. The governing equations of the self-powered thermoelectric car seat cooler are given by Equations (3. 16), (3. 17), (3. 24), and (3. 25). These equations apply to both power generation and to seat cooling.

3.5) Experimental Comparison

To determine the validity of the developed equations, the performance is compared to experimental results. Dias et al. built and tested a STEG similar in design to the self-powered thermoelectric car seat cooler [31]. The layout of the STEG from the experiment is shown in Figure 3. 9. It consists of an anodized aluminum plate inclined at an angle of 20°. Attached to the aluminum plate is the TEG and insulation. The TEG uses an aluminum heat sink to dissipate heat. Dias et al. include much information about the experiment such as the size and materials of many of the components used. The thermoelectric generator used in the setup is a TEG241-1.0-1.2 from EVERREDtronics Ltd. [32]. In the original experiment, Dias et al. were interested in the power output of the STEG over the course of a day. To study this, many measurements were made including the ambient temperature, the top plate temperature, the heat sink temperature, and the TEG voltage output over a 12 hour period.

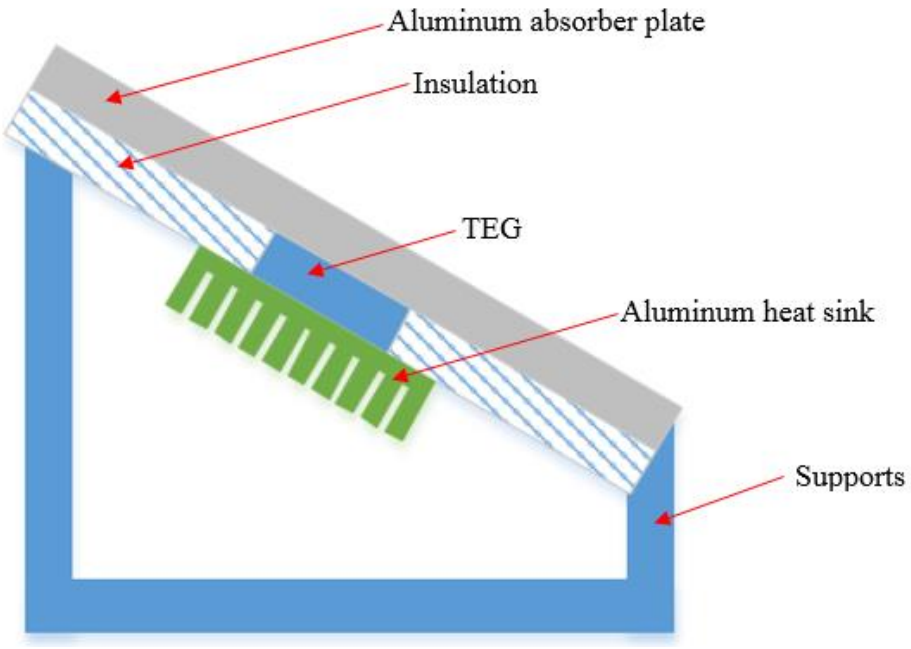

Figure 3. 9 Physical layout of STEG built by Dias et al.

3.6) Non-Dimensional Scheme

The following non-dimensional scheme is modified from a technique developed by Lee [16]. The non-dimensionalization of the governing equations is a powerful tool because it limits the total number of parameters which the designer must choose. Additionally, it allows the designer to see the effect specific factors have on the performance of the thermoelectric device. As long as the boundary conditions of the problem are defined, the optimization will return an optimal design. In this design, the dimensionless thermal conductance (N_k), dimensionless resistance (R_r), and dimensionless current (N_I), and dimensionless heat sink convection (N_{2c}) are optimized. Additionally, the effect of absorber plate area (A_{abs}) is studied.

The equations are non-dimensionalized with respect to the solar energy received on the top plate, $\alpha_{abs}\tau A_{abs}q_s''$. The dimensionless thermal conductance is given by

$$N_k = \frac{n\left(\frac{A}{L}\right) kT_{sur}}{\alpha_{abs}\tau_{glass}A_{abs}q_s''} \quad (3.\ 26)$$

which is the ratio of conducted energy to solar energy. The dimensionless convectance of the absorber plate is represented by

$$N_{1c} = \frac{A_{abs}h_{abs}T_{sur}}{\alpha_{abs}\tau_{glass}A_{abs}q_s''}. \quad (3.\ 27)$$

The dimensionless radiation of the conductive plate is given by

$$N_{1rad} = \frac{A_{abs}\epsilon_{1s}\sigma T_{sur}^4}{\alpha_{abs}\tau_{glass}A_{abs}q_s''}, \quad (3.\ 28)$$

while the dimensionless radiation of the heat sink is given by

$$N_{2rad} = \frac{A_{sink}\epsilon_{2s}\sigma T_{sur}^4}{\alpha_{abs}\tau_{glass}A_{abs}q_s''}. \quad (3.\ 29)$$

The dimensionless radiation exchange between the top and bottom plates of the thermoelectric device is given as

$$N_{12rad} = \frac{(A_{TEG} - 2nA_e)\epsilon_{12}\sigma T_{sur}^4}{\alpha_{abs}\tau_{glass}A_{abs}q_s''}. \quad (3.\ 30)$$

The non-dimensional convection of the heat sink is

$$N_{2c} = \frac{h_2 A_2 T_{sur}}{\alpha_{abs}\tau_{glass}A_{abs}q_s''}. \quad (3.\ 31)$$

The dimensionless current is defined as

$$N_I = \frac{\alpha I}{\left(\frac{Ak}{L}\right)}. \quad (3.\ 32)$$

The dimensionless load resistance is given as

$$R_r = \frac{R_L}{R_{TE}}, \quad (3.\ 33)$$

where R_{TE} is the resistance of the thermoelectric and R_L is the resistance of the attached load. The dimensionless figure of merit is represented by

$$ZT_{sur} = \frac{\alpha^2}{\rho k} T_{sur}. \tag{3. 34}$$

The dimensionless temperatures are defined as

$$T_1^* = \frac{T_1}{T_{sur}} \tag{3. 35}$$

and

$$T_2^* = \frac{T_2}{T_{sur}}. \tag{3. 36}$$

To quantify the performance of the thermoelectric generator and cooler, the efficiency and coefficient of performance are defined. The system efficiency is

$$\eta = \frac{\dot{W}}{\alpha_{abs}\tau_{glass}A_{abs}q_s''}, \tag{3. 37}$$

where $\dot{W}$ is the power generated. The thermoelectric generator efficiency is

$$\eta_{TEG} = \frac{\dot{W}}{\dot{Q}_1}, \tag{3. 38}$$

where $\dot{Q}_1$ is the heat into the thermoelectric. The COP of the thermoelectric cooler is given by

$$COP = \frac{\dot{Q}_1}{\dot{Q}_2 - \dot{Q}_1}, \tag{3. 39}$$

where $\dot{Q}_1$ is the cooling power and $\dot{Q}_2$ is the heat rejected by the thermoelectric.

Using these parameters, the governing equations can be rewritten in non-dimensional terms. The form of the equations are different however when considering

power generator versus cooling. For power generation, Equations (3. 16), (3. 17), (3. 24), and (3. 25) are represented as follows. For the top side of the thermoelectric,

$$\dot{Q}_1^* = 1 - N_{1rad}\left(T_1^{*4} - 1\right) - N_{12rad}\left(T_1^{*4} - T_2^{*4}\right) - N_{1c}(T_1^* - 1) \tag{3. 40}$$

and

$$\dot{Q}_1^* = N_k(T_1^* - T_2^*)\left[\frac{ZT_{sur}T_1^*}{R_r + 1} - \frac{ZT_{sur}(T_1^* - T_2^*)}{2(R_r + 1)^2} + 1\right]. \tag{3. 41}$$

For the bottom, the energy balance is

$$\dot{Q}_2^* = N_{2c}(T_2^* - 1) - N_{12rad}\left(T_1^{*4} - T_2^{*4}\right) - N_{2rad}\left(T_2^{*4} - 1\right) \tag{3. 42}$$

and

$$\dot{Q}_2^* = N_k(T_1^* - T_2^*)\left[\frac{ZT_{sur}T_2^*}{R_r + 1} + \frac{ZT_{sur}(T_1^* - T_2^*)}{2(R_r + 1)^2} + 1\right]. \tag{3. 43}$$

The equations for power generation include all the non-dimensional terms listed, except for N_I. The equations for cooling operation use both Equations (3. 40) and (3. 42). The equations for the thermoelectric are

$$\dot{Q}_1^* = N_k\left[N_I T_1^* - \frac{N_I^2}{2ZT_{sur}} + (T_1^* - T_2^*)\right]. \tag{3. 44}$$

and

$$\dot{Q}_2^* = N_k\left[N_I T_2^* + \frac{N_I^2}{2ZT_{sur}} + (T_1^* - T_2^*)\right]. \tag{3. 45}$$

For cooling, the equations use all the terms except for R_r.

When Equations (3. 41) through (3. 45) are used for optimizing either the generator or the cooler, the only unknowns are the temperatures at the top and bottom of the thermoelectric, T_1^* and T_2^*. Therefore when determining the performance of the cooler or the generator, there are two equations and two unknowns. Through use of a

nonlinear equation solver, the temperature of both sides of the thermoelectric can be found.

3.7) Optimization of Natural Convection Heat Sink

The heat sink used in this design utilizes natural convection to dissipate heat. Due to this, the design of the heat sink is limited by the geometrical layout. For specified conditions, an optimal design exists for the sink. A schematic of the finned heat sink is shown in Figure 3. 10. The following analysis uses parameters developed by Bar-Cohen and Rohsenow [33].

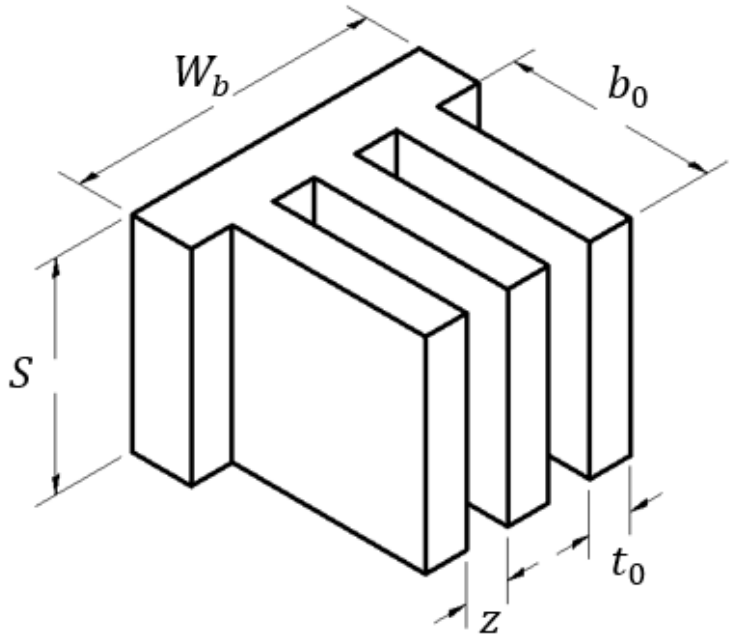

Figure 3. 10 Finned heat sink.

The Rayleigh number based on the length of the heat sink is found from

$$Ra = \frac{g\beta(\mathrm{T}_2 - T_{sur})S^3}{\omega\upsilon}, \tag{3. 46}$$

where g is the gravitational constant, β is the volumetric thermal expansion coefficient, T_2 is the base temperature of the heat sink, T_{sur} is the ambient temperature, S is the

length of the fin, ω is the thermal diffusivity of air, and υ is the kinematic viscosity of air. The optimal fin spacing is

$$z_{opt} = 2.714S * Ra^{\frac{-1}{4}}. \tag{3. 47}$$

The following Nussult correlation is used to calculate the heat transfer coefficient for natural convection cooling between two parallel vertical plates. This particular equation assumes symmetric isothermal plates with negligible plate thickness. The Nusselt number is given by

$$Nu = \frac{h_2 z_{opt}}{k_{air}} = \left[\frac{576}{El^2} + \frac{2.873}{El^{\frac{1}{2}}}\right]^{-\frac{1}{2}}, \tag{3. 48}$$

where El is the Elenbaas number and is defined as

$$El = \frac{g\beta(T_2 - T_{sur})z_{opt}^3}{\omega\upsilon}\frac{z_{opt}}{S}. \tag{3. 49}$$

The efficiency of a single fin can be determined from the following relation

$$\eta_{fin} = \frac{\tanh(mb_0)}{mb_0}, \tag{3. 50}$$

where m is defined as

$$m = \sqrt{\frac{2h_2^2(S + t_0)}{k_{al}St_0}}. \tag{3. 51}$$

The total number of fins is found using

$$n_{fin} = \frac{W_b}{z_{opt} + t_0}, \tag{3. 52}$$

where W_b is the width of the heat sink. The area of a single fin is

$$A_{fin} = 2(S + t_0)b_0. \tag{3. 53}$$

The total convective area of the heat sink is

$$A_{total} = n_{fin}\left[2(S + t_0)b_0 + Sz_{opt}\right]. \quad (3.\ 54)$$

The overall efficiency of the heat sink is

$$\eta_{total} = 1 - n_{fin}\frac{A_{fin}}{A_{total}}\left(1 - \eta_{fin}\right). \quad (3.\ 55)$$

Using the overall efficiency, the total heat transfer is

$$\dot{q}_{total} = \eta_0 h_z A_{total}(T_2 - T_{sur}). \quad (3.\ 56)$$

These relations, in conjunction with the non-dimensional equations, can be used to fully optimize the design.

3.8) Optimization Routine

The previous sections introduce several optimization equations. An organized routine is developed to compute and evaluate the ideal properties. This routine is shown in Figure 3. 11. The process begins by defining the constant properties for the materials used and the specific boundary conditions. Initial guesses of the optimal geometry are also specified. The system then sweeps through a range of absorber plate areas. At each area, the optimal values of N_k, R_r, N_{2c}, and N_I are found. This is accomplished by varying a single parameter over a range of values while holding all others constant. The value of the parameter which maximizes the either the generator output or the cooling performance is then recorded. This process is iterated until the values of N_k, R_r, and N_I converge to constant values. Once finished, the routine allows for visualization of the effect of absorber area on generator and cooler performance.

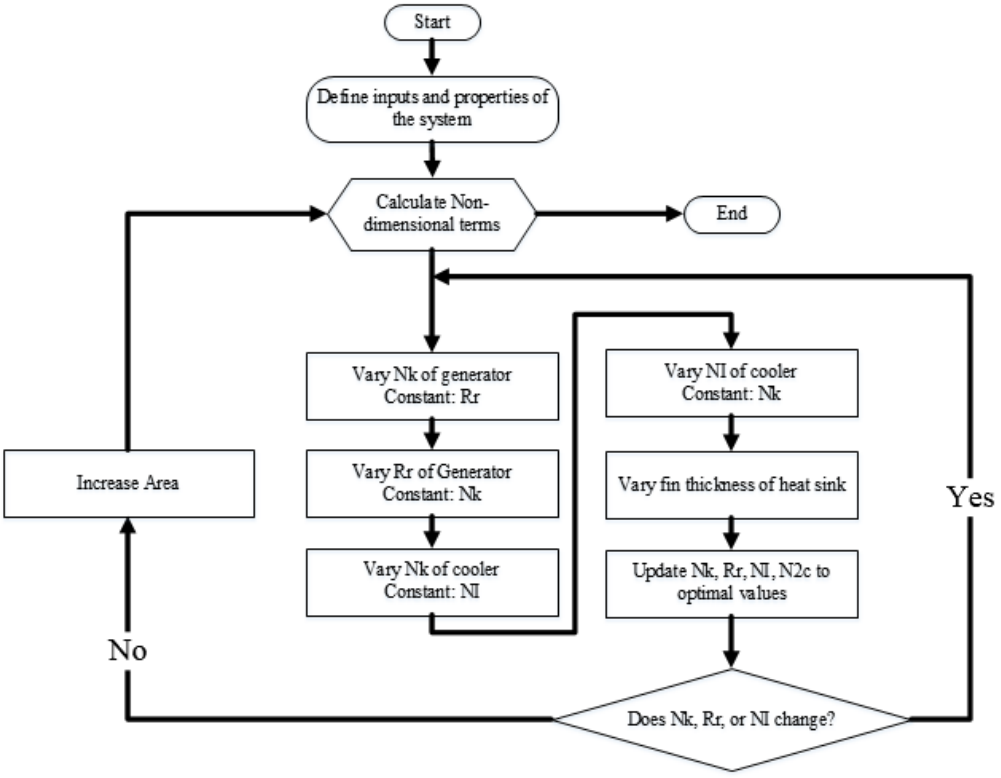

Figure 3. 11 Iterative optimization method.

3.9) Modeling Ambient Conditions

In order to make use of the governing equations, the boundary conditions must be known. These boundary conditions are the solar irradiance and the car interior temperature.

The behavior of solar irradiance throughout the day is determined by observing measured data. Elizabeth City College under the direction of the National Renewable Energy Laboratory (NREL) has measured solar irradiance for several years [34]. Data measured on July 1, 2012 at Elizabeth City, North Carolina is plotted in Figure 3. 12. The data begins at 6 AM, which corresponds to time 0 on the plot. Fitting a curve to the data, it is shown that a half sine wave closely models the solar irradiance for most of the day. There are a few deviations from this trend, but this is mostly due to cloud cover. In

the afternoon the sun begins to set and the solar data deviates from the model. This is accounted for in the final model by cutting the sine wave short at this time. Using this relation, the only parameters which the solar model needs is the maximum solar irradiance for the particular day and the time of sunset. Therefore, the model for solar irradiance is

$$q''_{solar} = q''_{max} * \sin\left(\frac{t\pi}{12}\right), \tag{3. 57}$$

where q''_{max} is the maximum expected solar irradiance in W/m^2 and t is the time in hours. As noted above, this model is only valid from 6 AM to 3 PM. After 3 PM, the solar irradiance drops off rapidly to zero.

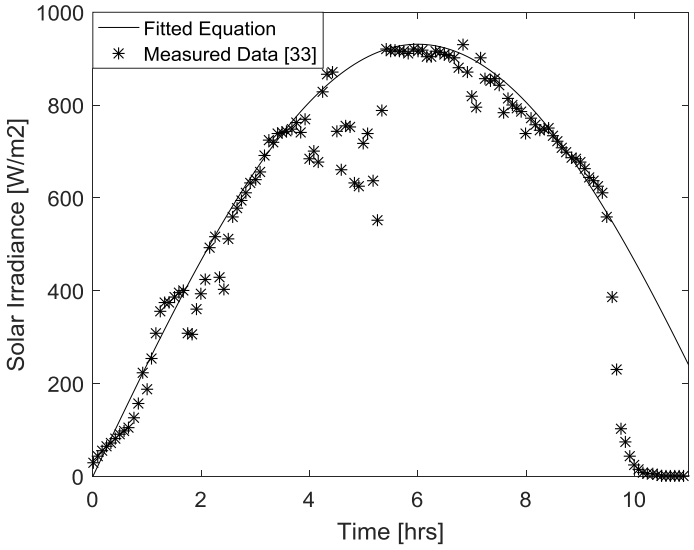

Figure 3. 12 Solar irradiance data measured by Elizabeth City College on July 1, 2012 [34].

The variation of the car interior temperature is studied by Dadour et al. [11]. This study attempts to construct a model of the car interior temperature variation throughout the day. Although the model developed by Dadour et al. shows good correlation, the specific values used are not given. However, the experimental results provide insight

into the thermal behavior of the car interior. The first major take away is that while the air temperature outside the car may experience slight variation throughout the day, the interior air temperature follows a steady pattern. Second, the interior temperature seems to be more correlated to the solar irradiance than to the outdoor temperature. The interior temperature has a sinusoidal time dependence similar to the solar irradiance pattern. Therefore, the model of the interior car air is also a half sine wave.

While the results recorded by Dadour et al. provide a qualitative prediction of the car interior temperature, it does not provide any quantitative values. This is found from a study by Grundstein et al. who created an equation to predict the maximum daily car interior temperature [35]. For the experiment a metallic gray 2005 Honda Civic was parked in an open lot with direct exposure to the sun. The interior temperature of the car was measured by a temperature probe suspended 150 mm from the ceiling. Ambient temperature and solar data were taken from a local weather station 125 m away from the car. Data was recorded for 58 days. The equation for the car maximum cabin temperature is

$$T_{max} = 0.036 * \bar{q}'' + 1.02 * T_{ambient} + 8.8, \tag{3. 58}$$

where $\bar{q}''$ is the average solar irradiance in W/m^2 and $T_{ambient}$ is the maximum exterior air temperature in $°C$ [35]. This equation accounts for 80% of the variability in the experimental measurements and has a root mean squared error (RMSE) of 3.7 [35]. Using the maximum temperature from Equation (3. 58) and the information from the study by Dadour et al., the equation for the interior temperature of the car is

$$T_{sur} = (T_{max} - T_{min}) * \sin\left(\frac{t\pi}{12}\right) + T_{min}, \tag{3. 59}$$

where t is the time of day in hours and T_{min} is the minimum outdoor temperature. The minimum outdoor temperature could also be thought of as the starting temperature of the car model. An example plot of interior temperature variation of the car is given in Figure 3. 13.

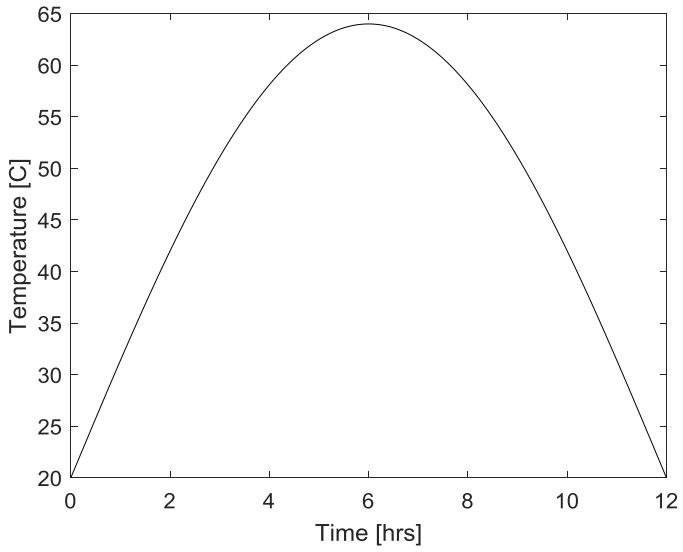

Figure 3. 13 Temperature variation of car interior air.

For this model, the maximum outdoor temperature is $30°C$ and the minimum is $20°C$. The average solar irradiance is from the curve in Figure 3. 12 and is 504 W/m^2. This results in a maximum car interior temperature of $57.5°C$.

Given the models of Equations (3. 57) and (3. 59), the inputs necessary for the thermoelectric equations developed are all known. Therefore, design and optimization of the device can begin.

Chapter 4: Results and Discussion

4.1) Validity of the Governing Equations

The validity of the governing equations developed in Section 3.4) are tested by comparing them to experimental data recorded by Dias et al [31]. This is done by inputting the relevant dimensions and properties of the experiment into the governing equations. The values used for this analysis are given in Table 4. 1. Several assumptions are made about the setup. The emissivity and absorptivity of the absorber are estimated from tabular data for anodized aluminum [36]. The heat sink is assumed to be made of anodized aluminum and the surroundings are assumed to be black body. The thermoelectric material properties are found for nanocomposite p-type Bi_2Te_3 at 311 K [27,28]. This temperature is the average of the hot and cold side between hours 9 and 15 of the experimentally measured temperatures.

Table 4. 1 Given and Estimated Parameters for the STEG Experiment by Dias et al.

Description and symbol	Value	Description and symbol	Value
Area of absorber, A_{abs}	0.16 m^2	Emissivity of absorber, ϵ_{1rad}	0.84 (estimated)
Absorptivity of absorber, α_{abs}	0.17 (estimated)	Emissivity of surroundings, ϵ_{sur}	1 (estimated)
Radiative area of heat sink, A_{1rad}	0.0016 m^2	Emissivity of sink, ϵ_{2rad}	0.84 (estimated)
Area of TEG leg, A	1.2 x 1.2 mm^2	Emissivity of ceramic TEG plates, ϵ_1, ϵ_2	0.1 (estimated)
Length of TEG leg, L	1 mm	Seebeck coefficient, $\alpha_p = -\alpha_n$	1.92e-04 V/K
Number of pairs of legs, n	241	Electrical resistivity, $\rho_p = \rho_n$	8.45e-06 Ωm
Area of TE ceramic plate, A_{TE}	0.0016 m^2	Thermal conductivity, $k_p = k_n$	1.08 W/m^2K
Electrical resistance ratio, R_r	0.25	Convective coefficient of absorber plate, h_1	3.6 W/m^2K (estimated)
Maximum solar irradiance, q''_{solar}	1200 W/m^2 (estimated)	Thermal resistance of heat sink, R_{sink}	0.33 K/W

The average convective coefficient of the absorber plate is determined from Nusselt number correlations for natural convection of horizontal plates by Lloyd et al. [37]. The net emissivity between the ceramic plates of the TEG is given by

$$\epsilon_{12rad} = \frac{1}{\frac{1}{\epsilon_1} + \frac{1}{\epsilon_2} - 1} = 0.053, \tag{4. 1}$$

where ϵ_1 is the emissivity of the top plate and ϵ_2 is the emissivity of the bottom plate. The solar irradiance is the only input not given. This is simulated using the model developed in Section 3.9) and is shown in Figure 4. 1.

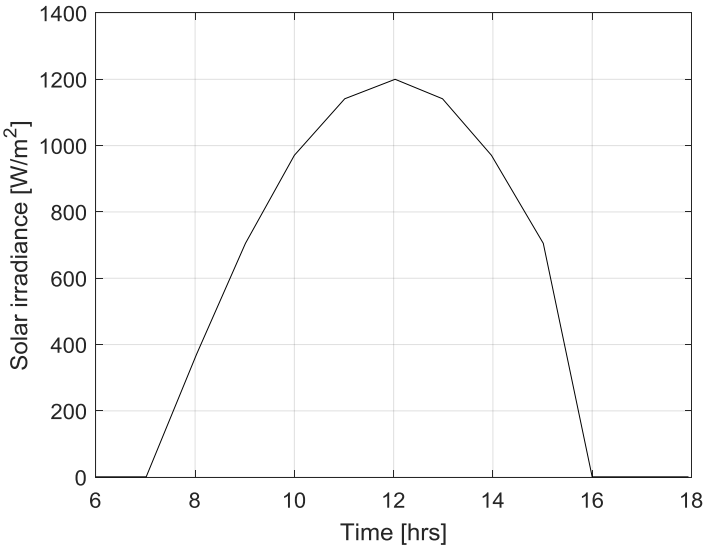

Figure 4. 1 Estimated solar irradiance for the experimental STEG.

By inputting this solar irradiance data to the model, the hot and cold side temperatures of the thermoelectric are predicted. Figure 4. 2a and Figure 4. 2b compare the analytical and experimental temperatures. As shown, there is good agreement between the two.

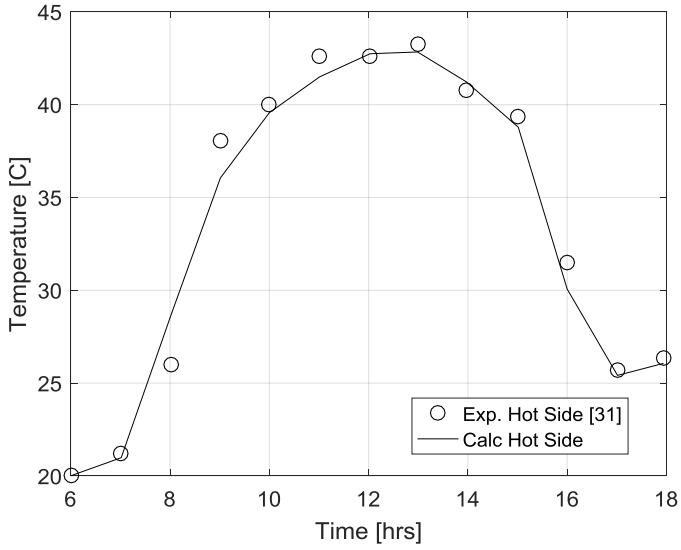

(a)

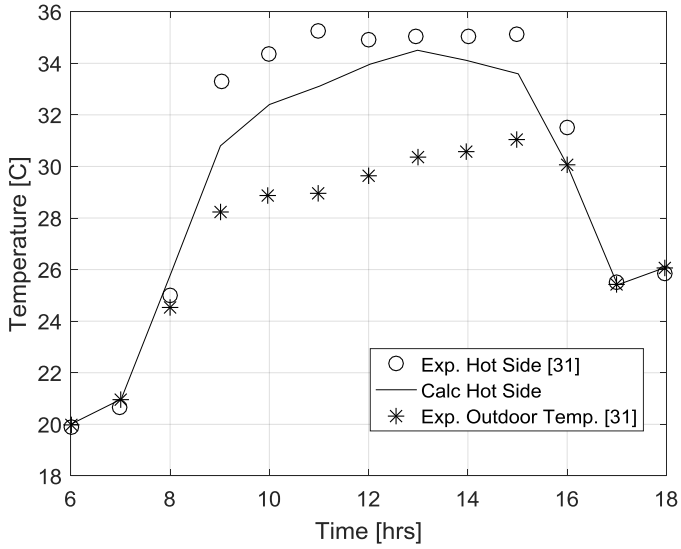

(b)

Figure 4. 2 Simulated output of 1D equations vs experimental results for (a) absorber side temperature and (b) heat sink temperature.

The resulting voltage produced by the TEG is shown in Figure 4. 3. Like the temperature plot, there is good agreement between the experimental and calculated values.

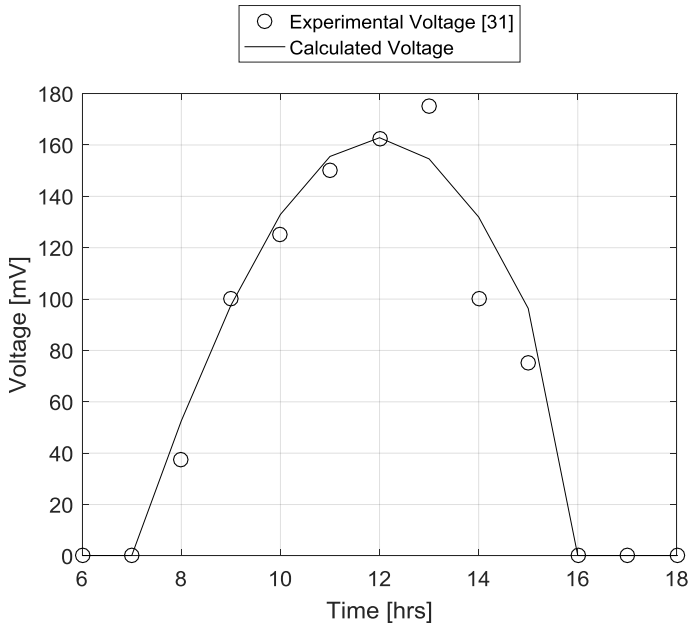

Figure 4. 3 Voltage output of the analytical model vs the experimental results.

One point to note is that the thermoelectric equations derived in Section 3.4) are for steady state conditions. However the analysis above is a transient problem. There are two justifications for using the steady state equations as such. First, the thermal conductivity of the device is relatively high and the mass is small. Therefore, under set boundary conditions, it does not take long for the system to come to steady state. The second reason for a steady state assumption is the large time span involved. For this study, the time frame is in hours. When the external conditions change the transients constitute a small portion of the total result.

Because there is good agreement between the 1D analytical model and the experimental results, it is concluded that the model can reasonably predict the performance of the self-powered thermoelectric car seat cooler.

4.2) Non-dimensional Optimization Results

The next section details the full design optimization. This involves the use of the routine described in Section 3.8) and the non-dimensional equations developed in Section 3.6). The design parameters are given in Table 4. 2. An initial guess of parameters to be optimized are needed to start. These include N_k, R_L, N_I, and R_{sink}.

Table 4. 2 Parameters Used in the Design of the Self-powered Thermoelectric Car Seat Cooler

Description and symbol	Value	Description and symbol	Value
Absorptivity of absorber, α_{abs}	0.9	Transmittance of windshield glass, τ_{glass}	0.76
Radiative area of heat sink, A_{2rad}	0.0016 m^2	Emissivity of absorber, ϵ_{1rad}	0.3
Number of pairs of legs, n	121	Emissivity of surroundings, ϵ_{sur}	1
Area of TE ceramic plate, A_{TE}	0.0016 m^2	Emissivity of sink, ϵ_{2rad}	0.84
Maximum solar irradiance, q''_{solar}	1000 W/m^2	Emissivity of ceramic TEG plates, ϵ_1, ϵ_2	0.1
Average solar irradiance, $q''_{solar,avg}$	541 W/m^2	Seebeck coefficient, $\alpha_p = -\alpha_n$	2.07E-04 V/K
Sunset	3:00 PM	Electrical resistivity, $\rho_p = \rho_n$	1.08E-05 $\Omega\, m$
Minimum outdoor temperature, T_{min}	20°C	Thermal conductivity, $k_p = k_n$	1.02 W/m^2K
Maximum outdoor temperature, T_{max}	35°C	Convective coefficient of absorber plate, h_1	3.6 W/m^2K
Average interior temperature, T_{avg}	48.8°C	Thermal resistance of heat sink, R_{sink}	20 K/W
Length of heat sink, L_b	0.04 m	Thermal diffusivity of air, ω	26.08E-06 m^2/s
Width of heat sink, W_b	0.04 m	Kinematic viscosity of air, υ	18.31e-06 m^2/s
Height of heat sink, b_0	0.04 m	Thermal conductivity of air, k_{air}	28.08e-03 W/m^2K
Thermal resistance ratio, N_k	3	Volumetric thermal expansion of air, β	0.0031 K^{-1}
Electrical resistance ratio, R_r	1.5	Thermal conductivity of aluminum, k_{al}	177 W/m^2K
Dimensionless current, N_I	1	Gravitational constant, g	9.81m/s^2

The absorptivity of the absorber plate is increased compared to that of Section 3.1). The reason for this is to increase the hot side temperature of the plate which should also increase the power output of the generator. This is achieved by painting the absorber

black [36]. The maximum solar irradiance is set to 1000 W/m^2 and the outdoor temperature is set to begin at 20°C and peak at 35°C. These values are typical for the eastern United States during the summer months [34]. A plot of the solar model is given in Figure 4. 4. The thermoelectric property values are found assuming nanocomposite p-type Bi_2Te_3 at a temperature of 354 K [27,28]. This is the average temperature of the hot and cold sides at the optimal cooling temperature. This temperature is found iteratively. Various properties of air and aluminum are also given to optimize the natural convection of the heat sink. These values are evaluated at the average interior car temperature, T_{avg} [36]. The transmittance of the windshield glass is typical of most cars [12].

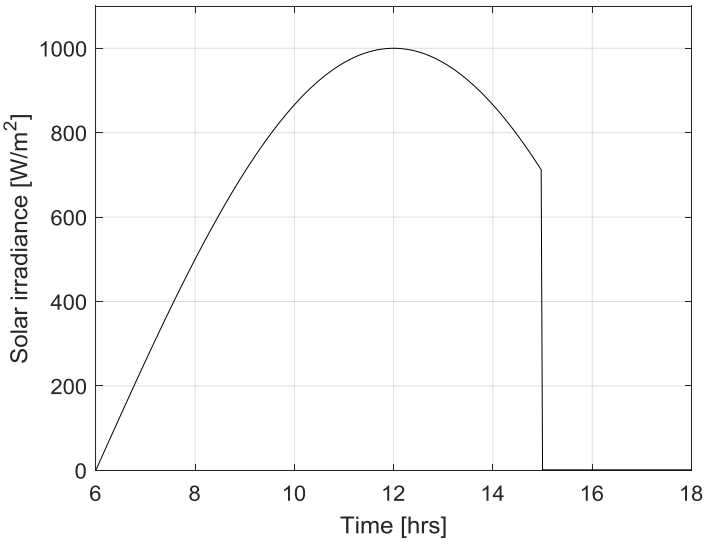

Figure 4. 4 Solar input used to determine optimal parameters and performance.

One important point to emphasize for the optimization routine used here is that it will only find the optimal parameters for fixed boundary conditions. However, during the course of the day the boundary conditions will vary as the interior temperature and the solar irradiance change. To ensure a robust design, the device is optimized with respect

to the average solar irradiation and the average interior car temperature. These averages are determined from the models developed in Section 3.9).

The first parameter considered is the area of the absorber. The variation in dimensionless cooling temperature and seat temperature with absorber area is shown in Figure 4. 5a. In Figure 4. 5 the effect of absorber area on power generated is plotted.

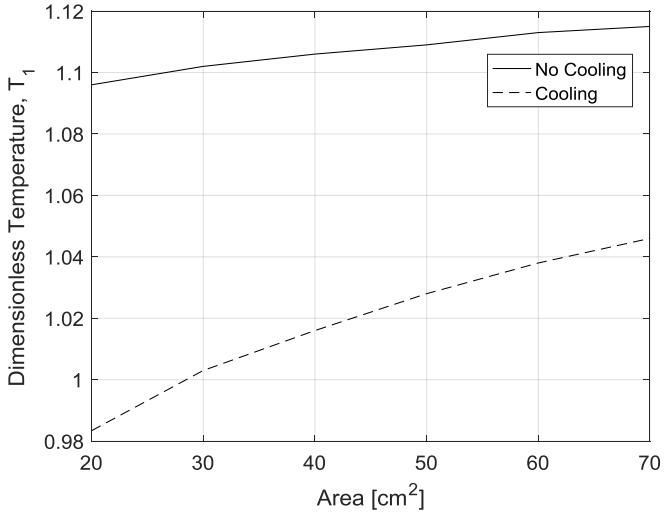

(a)

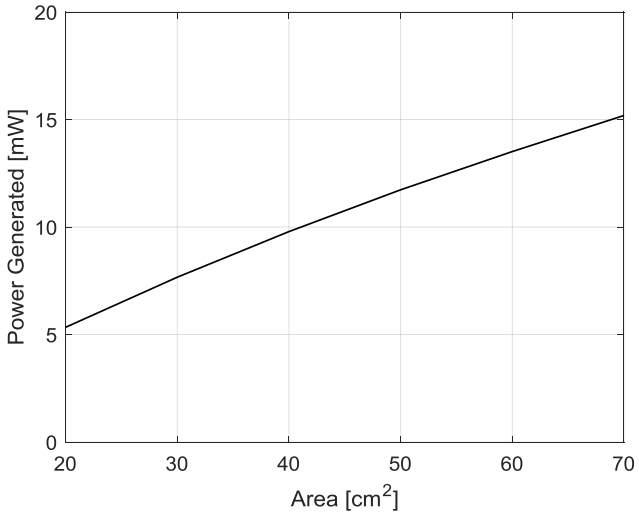

(b)

Figure 4. 5 Effect of absorber area on (a) dimensionless temperature and (b) power output.

In Figure 4. 5a there are two lines plotted. The first is "No Cooling", which denotes the temperature of the absorber plate with the thermoelectric cooler turned off. "Cooling" denotes the temperature of the absorber plate with the thermoelectric cooler on operating at maximum cooling. Both of the temperatures displayed are non-dimensionalized with respect to the ambient temperature of the car. Therefore, 1 on the axis denotes the ambient temperature. The last value is the power output of the thermoelectric generator at the average conditions. It is seen that as area increases, the power generated increases. This is because more solar energy is being absorbed which leads to a higher temperature difference. But, as the absorber area increases, the cooling performance is reduced. Not only does the minimum temperature the device can cool to increase, but also the ΔT between no cooling and cooling decreases. Due to the larger area, more energy is gained from solar irradiance and from surroundings through radiation and convection, increasing the temperature. The ideal area is the point where the minimum acceptable cooling temperature is achieved. For this study, the desired cooling is chosen to be $25°C$ below the normal absorber temperature at average conditions. However, another cooling point could be chosen, but this is up to the designer. Using this value, the optimal area for the design is 0.006 m^2 which is a square plate that is 7.7 cm x 7.7 cm. The optimal design values found at this area are displayed in Table 4. 3.

Table 4. 3 Optimal Non-dimensional Design Parameters

Parameter	Optimal value
A_{abs}	0.006 m^2
N_k	4.6
R_r	1.7
N_I	0.375
N_{2c}	11.095

To demonstrate that these values are indeed the optimal, Figure 4. 6 through Figure 4. 11 are provided. In Figure 4. 6, the effect of load resistance on power generation and TEG efficiency is shown. The maximum efficiency and power output are very close to each other. The ideal value of R_r is chosen according to maximum power. Also of note in this plot is that increasing the resistance ratio does not drastically impact generator performance. Decreasing the ratio however severely reduces the power output.

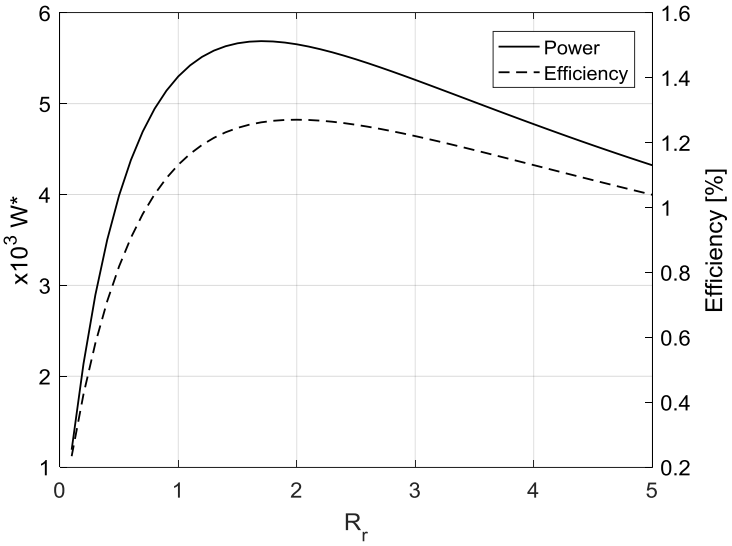

Figure 4. 6 Change in dimensionless power and efficiency as R_r varies.

In Figure 4. 7 the relationship between dimensionless power and efficiency is shown. There is an obvious optimal value of N_k for power generated, but for not for efficiency.

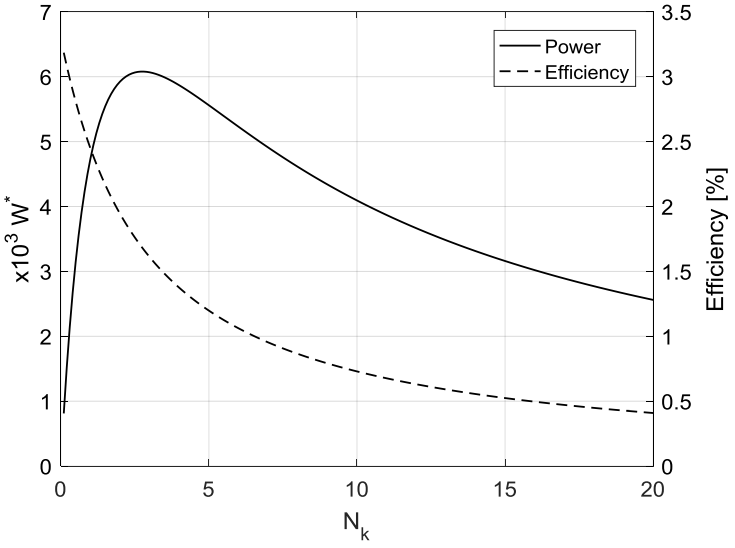

Figure 4. 7 Variation in dimensionless power and efficiency as N_k varies.

Next are the performance curves for the cooling operation. In both Figure 4. 8 and Figure 4. 9 the variance of COP and cooling power are shown. In Figure 4. 8 the effect of N_I is examined. It is seen that there is an optimal cooling value for a specific current input. The COP varies with current by starting at large values near small current input and decreasing as current increases. A large COP could be achieved by using a small input current, but this would produce very little cooling. To achieve maximum cooling, the optimal current is chosen with respect to cooling power. Figure 4. 9 examines the effect of N_k on cooling performance. As typical of the other plots up to this point, there is a clear optimal value.

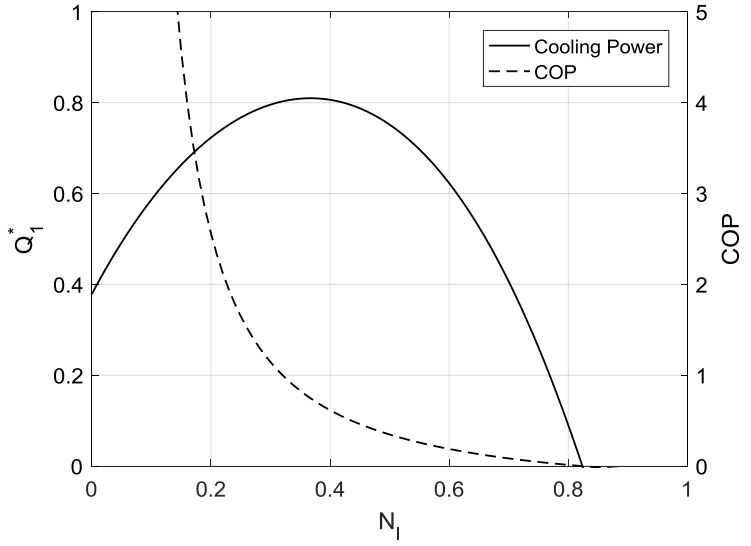

Figure 4. 8 Change in COP and dimensionless cooling power as N_I varies.

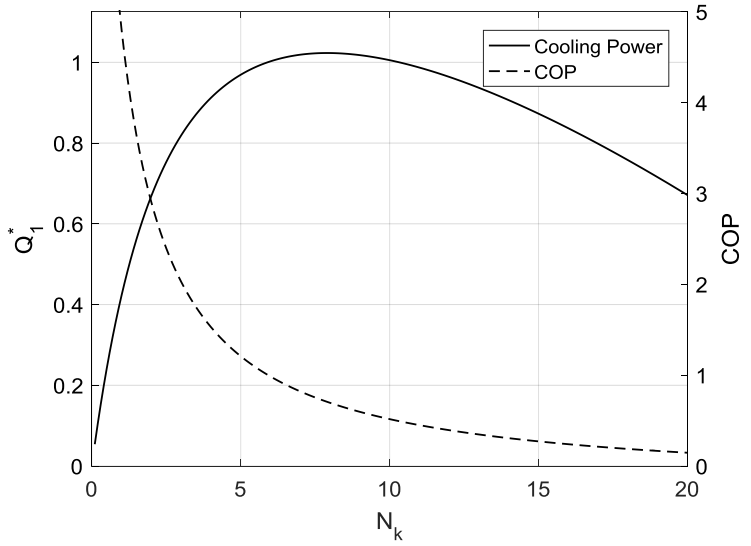

Figure 4. 9 Change in COP and dimensionless cooling power as N_k varies.

The optimization of N_k is different from that of N_I and R_r. Like the absorber area, N_k affects both power generation and cooling performance. This variation is shown in Figure 4. 10. It is important to note the variance in the optimal value of N_k for both operations. The definition of the dimensionless thermal conductance is given in Equation (3. 26). The two important parameter in this equation are the number of thermoelectric

leg pairs and the ratio of leg area to leg length. Generators prefers a smaller N_k while coolers prefers a larger value. Considering the number of legs is constant, the previous statement physically means that in general, the generator performs better with longer legs that have small areas. The reason for this is that long, slim legs allow for a larger temperature difference which leads to higher power output. However, this is only valid up to a certain point as it also increases the electrical resistance, which reduces power. Conversely, the cooler operates better with short legs with larger cross sectional areas. This reduces the Joule heating in the leg, but will allow thermal energy from the hot side to travel back to the cold side. Without the curves, it would be difficult to determine how to balance these concerns. To determine the best compromise between cooling and power, the curves are normalized on a scale from zero to one and then added together according to

$$Normalized\ Curve = \frac{N_{k,cooling}}{N_{k,cooling,max}} + \frac{N_{k,power}}{N_{k,power,max}}. \quad (4.\ 2)$$

Using this relationship, the ideal value of N_k occurs at the maximum value of the normalized curve. The result is shown in Figure 4. 11.

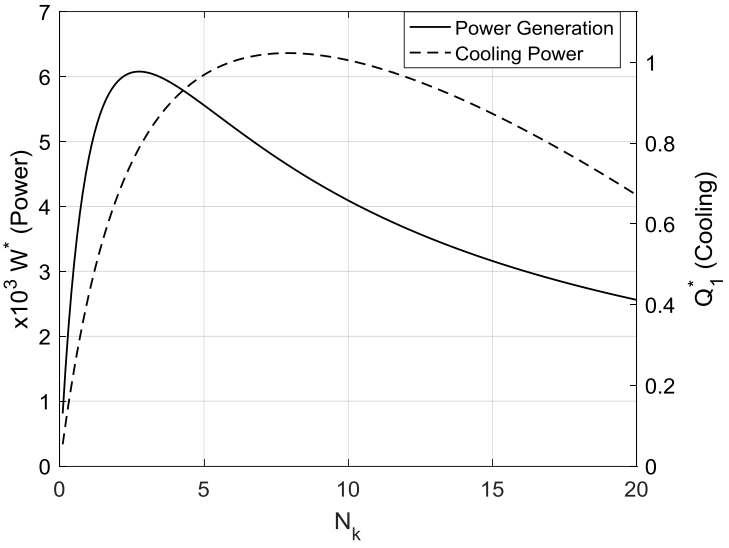

Figure 4. 10 Change in dimensionless power and dimensionless cooling power as dimensionless thermal conductance varies.

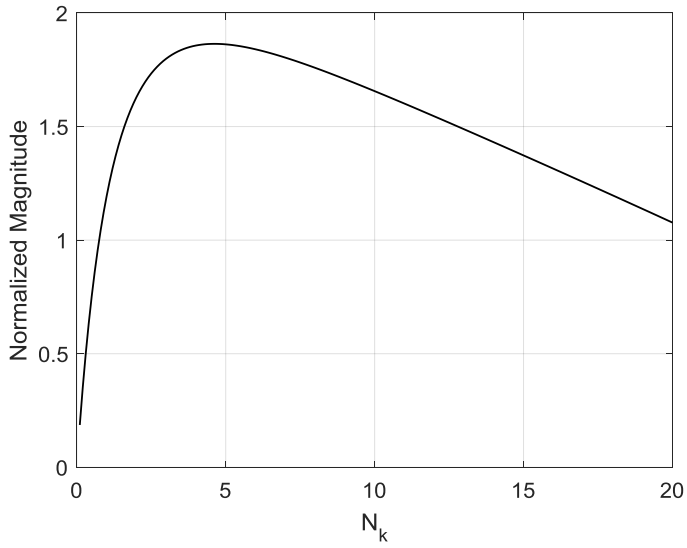

Figure 4. 11 Normalized sum of dimensionless power generation and cooling power as dimensionless thermal conductance varies.

4.3) Recommended Design

Given the optimal non-dimensional values, the complete design is fully described. The final design values are displayed in Table 4. 4 below. One value to note is the number of legs used. Varying the number of legs has no impact on the overall power

generated or cooling capacity of the self-powered thermoelectric car seat cooler as long the dimensionless values are kept constant. It does however affect the voltage and current produced. As the number of legs increases, the voltage increases and the current decreases. The value chosen for the number of legs is typical of commercially available thermoelectrics.

Table 4. 4 Optimal design parameters

Description and symbol	Value	Description and symbol	Value
Area of absorber, A_{abs}	0.006 m^2	Length of heat sink, L_b	0.04 m
Area of TEG leg, A	0.38 x 0.38 mm^2	Width of heat sink, W_b	0.04 m
Length of TEG leg, L	1 mm	Height of heat sink, b_0	0.04 m
Number of pairs of legs, n	121	Thickness of fins, t_0	0.5 mm
Area of TE ceramic plate, A_{TE}	0.0016 m^2	Spacing of fins, z_0	7.8 mm
Electrical resistance ratio, R_r	1.7	Number of fins, n_{fin}	4
		Heat sink performance, $\eta h_2 A_2$	0.0768 W/m^2K

With the full design of the device complete, the performance of the final product is evaluated.

4.4) Performance of Device

To gauge whether the self-powered thermoelectric car seat cooler is feasible, it is simulated over the course of an entire day. This analysis is similar to that in Section 4.1). The inputs to the model are the maximum solar irradiance, the minimum outdoor temperature, and the maximum outdoor temperature. The property values used are the same as those given in Table 4. 2. The results of the full day analysis are shown below. Figure 4. 12 displays the temperature variation of the surfaces of the thermoelectric generator and the interior car temperature. The hot side reaches a maximum temperature of about 112°C, the cold side 87°C, and the interior air reaches a maximum temperature

around $64°C$. In this simulation, the hot and cold sides of the generator fall to the temperature of the interior air once the absorber is no longer receiving sunlight. While in reality there may still be a temperature difference between the two sides after this point, any energy which may be generated from this is neglected. Figure 4. 13 plots the total power output throughout the day.

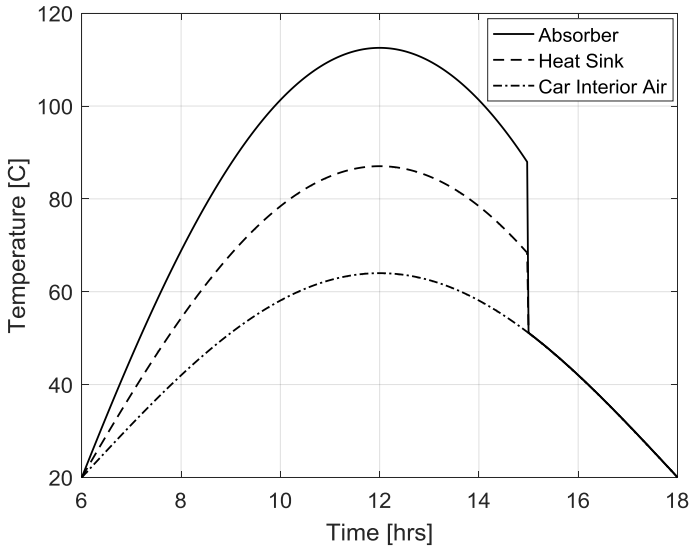

Figure 4. 12 Temperature variation throughout the day.

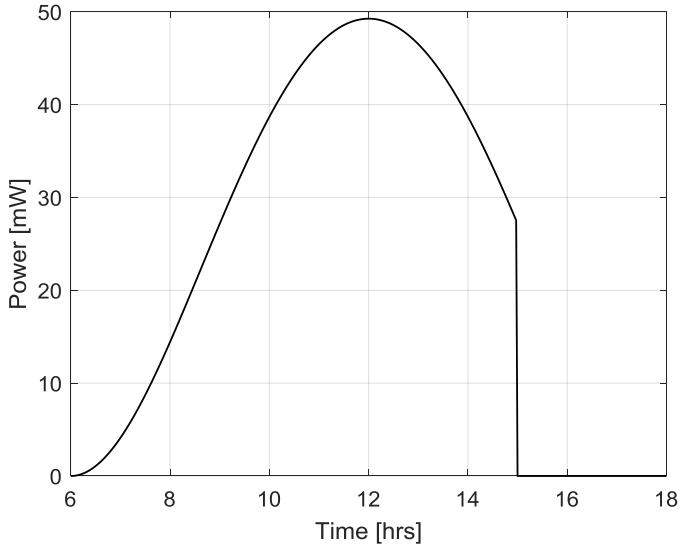

Figure 4. 13 Power output

The maximum power output is 49 mW and the total power generated is 1000 J. The maximum system efficiency is 1% and the maximum TEG efficiency is 2.4%. The voltage and current are shown in Figure 4. 14. This shows that the maximum voltage is 1.21 V and the maximum current is 40 mA.

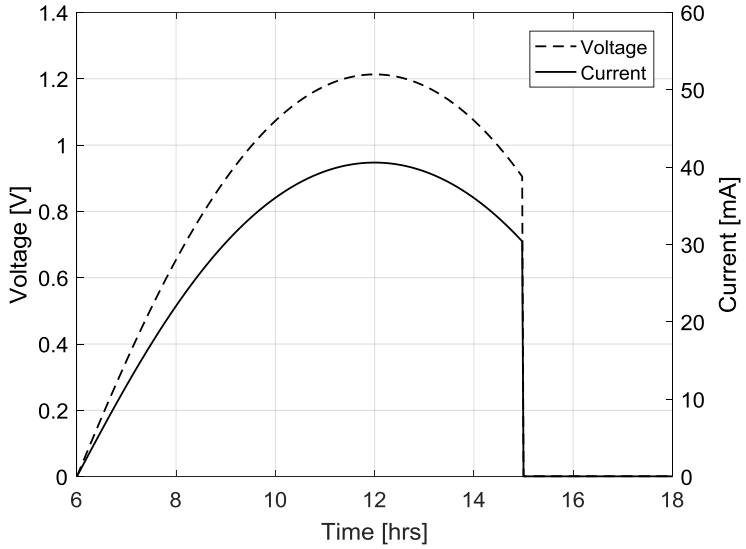

Figure 4. 14 Voltage and current variation

Lastly, the performance of the thermoelectric in cooling operation is plotted in Figure 4. 15 and Figure 4. 16. Shown in Figure 4. 15 is the variation of the hot and cold side temperatures as the supplied current is varied. The loading of this specific case is for the average solar irradiance and interior car temperature, which are 541 W/m^2 and 48°C. Under these conditions, the seat cooler reduces the temperature to 59.5°C, a 25°C temperature drop, which meets the design criteria set forth in Section 4.2). In Figure 4. 16 the cooling and heating power are shown. The cooling power refers to the heat removed from the absorber plate. The heating power refers to the heat dissipated by the heat sink. At maximum cooling, the device provides 1.8 W of cooling. A current of 0.24 A is supplied which results in a total power draw of 2.39 W for the device.

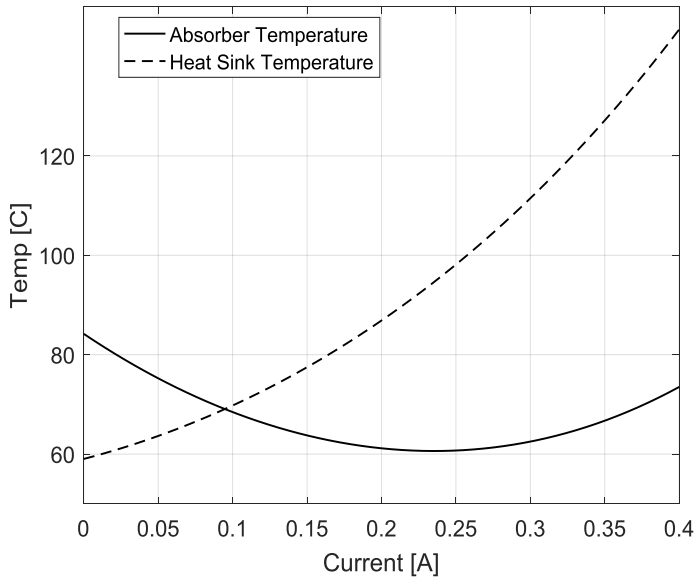

Figure 4. 15 Cooling temperature as a function of current for $\dot{Q}_{solar} = 541\ W/m^2$ and $T_{sur} = 48.8°C$.

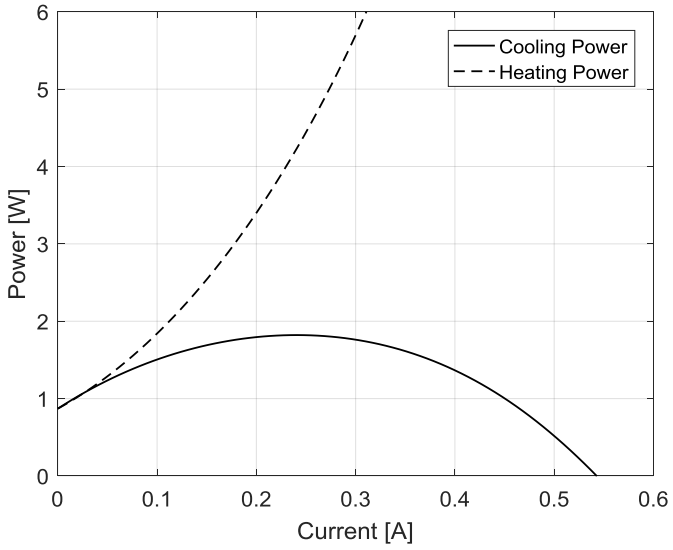

Figure 4. 16 Cooling power as a function of current for $\dot{Q}_{solar} = 541\ W/m^2$ and $T_{sur} = 48.8°C$.

With this information, it is possible to determine the feasibility of the design. With a total power of 1000 J, the cooler can operate at 0.24 A and 2.39 W for about 7 minutes. Looking into the transient behavior of thermoelectric coolers, Cheng et al. determined that at low current (0.5 A) a TEC will reach steady state at around 200 seconds [38]. Therefore, the seat cooler has enough energy to reach the steady state temperature before running out of power.

The loading shown in Figure 4. 15 and Figure 4. 16 is for the case of average solar irradiance and average interior car temperatures. Under more ideal circumstances, the self-powered thermoelectric car seat cooler can operate for longer and achieve lower temperatures. Suppose the vehicle owner returns sometime in the afternoon around 5:00 PM. According to the solar model, solar irradiance is negligible at this time and the interior car temperature is $31°C$. The temperature and cooling performance is given in Figure 4. 17 and Figure 4. 18.

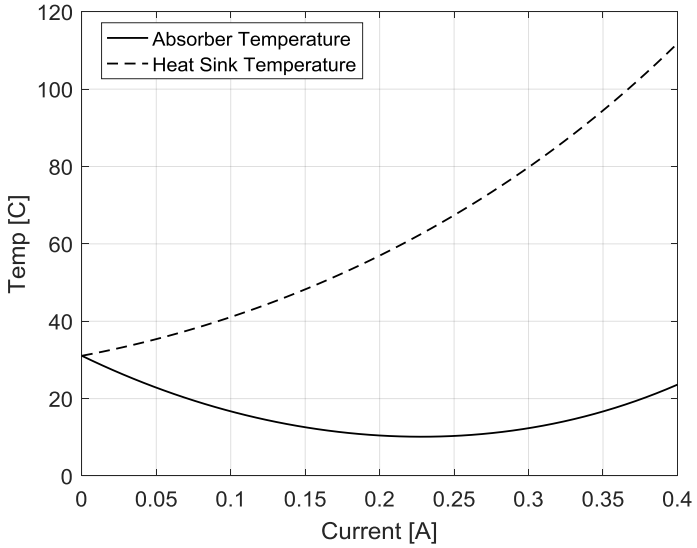

Figure 4. 17 Cooling temperature as a function of current for $\dot{Q}_{solar} = 0\ W/m^2$ and $T_{sur} = 31°C$.

The cooler is able to reduce the seat temperature to $10°C$ and provides 0.7 W of cooling.

At the minimum temperature, the cooler draws 2.3 W and can operate for 7.2 minutes.

This shows that the cooler is versatile and can operate under many different conditions.

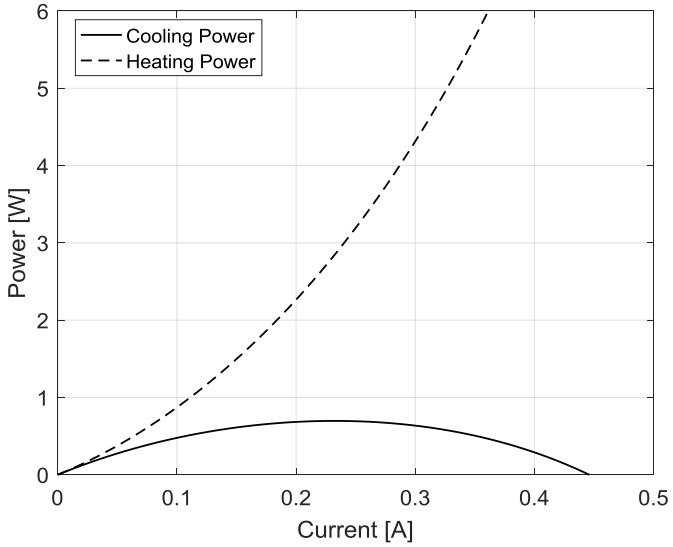

Figure 4. 18 Cooling power as a function of current for $\dot{Q}_{solar} = 0\ W/m^2$ and $T_{sur} = 31°C$.

The design of the self-powered thermoelectric seat cooler is fully detailed and the predicted performance is displayed. It is shown that under average loading conditions the seat is able to decrease the temperature to the desired temperature and the generator provides enough energy to do so.

4.5) ANSYS Model

To further support the analysis of Section 4.4), an ANSYS simulation of the thermoelectric device is presented using the thermal-electrical analysis tools. The advantage of ANSYS over the ideal equations is it can account for the variation of material properties with temperature. The material properties used are the same as those of Figure 3. 2. A model of the device geometry is shown below in Figure 4. 19.

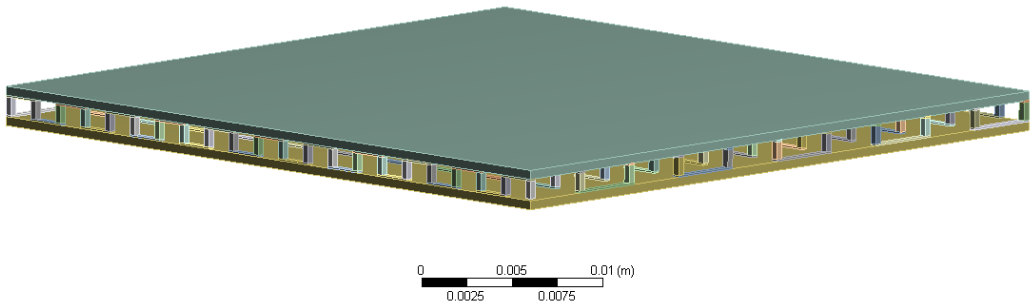

Figure 4. 19 Model of thermoelectric generator in ANSYS.

To model the performance, the top and bottom of the device are loaded to the same temperature variation as given in Figure 4. 12. A resistive element is attached in series to the thermoelectric generator to provide the optimal loading. The resulting power, current, and voltage predicted by ANSYS are compared to the ideal equations in Figure 4. 20, Figure 4. 21, and Figure 4. 22. There is slight difference between voltage and current output for each model. Excluding the first two hours, the maximum error between the two methods is 12% for the current and 13% for the voltage outputs. The

maximum error between the power outputs is 10%. The total energy generated according to ANSYS is 1040 J, which is just slightly higher than the 1000 J predicted by the ideal equations.

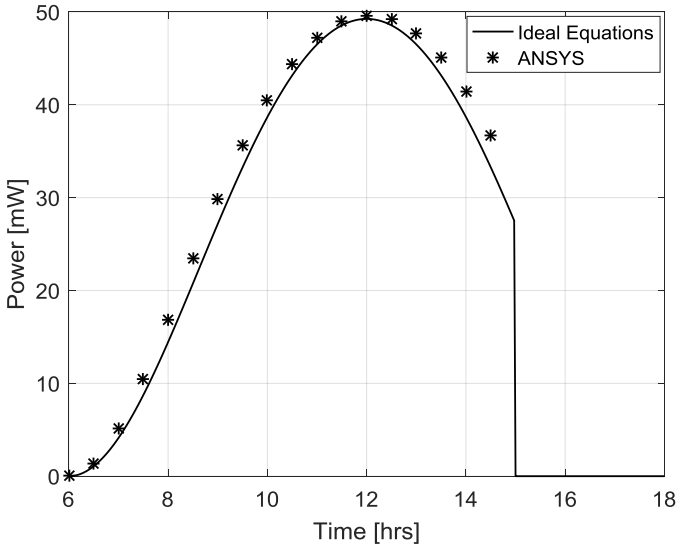

Figure 4. 20 Predicted power output from ANSYS and the ideal equations.

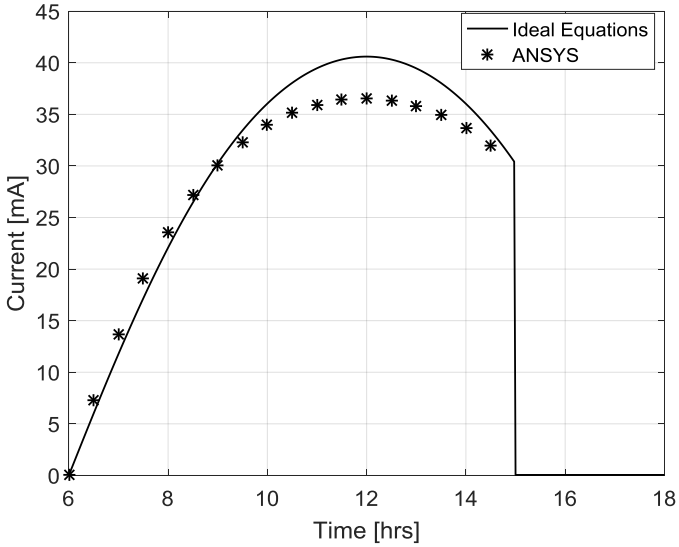

Figure 4. 21 Predicted current output from ANSYS and the ideal equations.

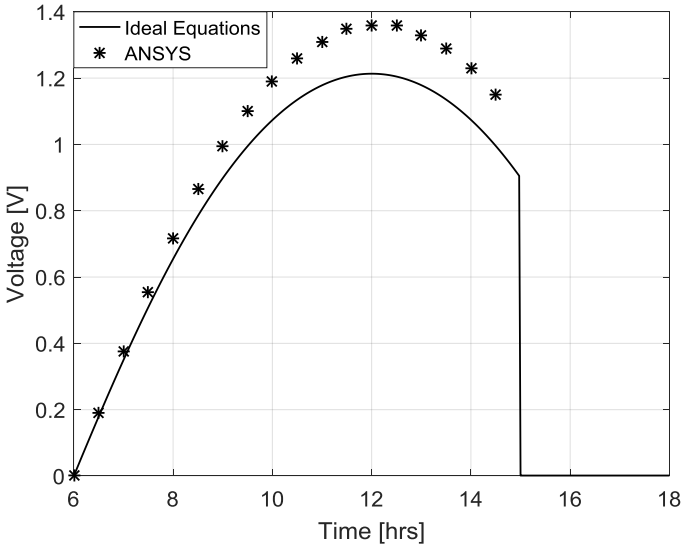

Figure 4. 22 Predicted voltage output from ANSYS and the ideal equations.

Likewise, the cooling performance is modeled in ANSYS. The model of one of the leg pairs is shown in Figure 4. 23.

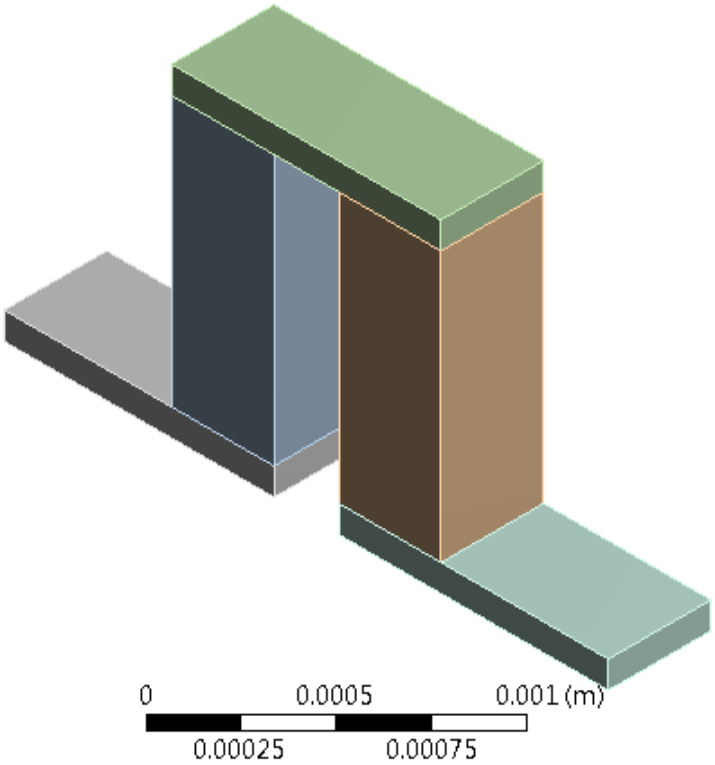

Figure 4. 23 Model of thermoelectric leg pair in ANSYS.

As with the generator, the top and bottom surfaces are set to the temperature specified in the curves given by the ideal equations. Then, the supplied current to the TEC is varied. From this, the power released and absorbed by the hot and cold junctions is recorded. This case models the cooling performance shown in Figure 4. 15 when the cooler operates at the average loading conditions. The results from ANSYS, shown in Figure 4. 24, are in agreement with the ideal solution. The cooling power predicted by ANSYS is slightly higher than that of the ideal equations. This is due to the Thomson effect, which increases the cooling power. Also, the two curves begin to deviate from one another at higher currents. This is to be expected and was predicted in Section 3.2).

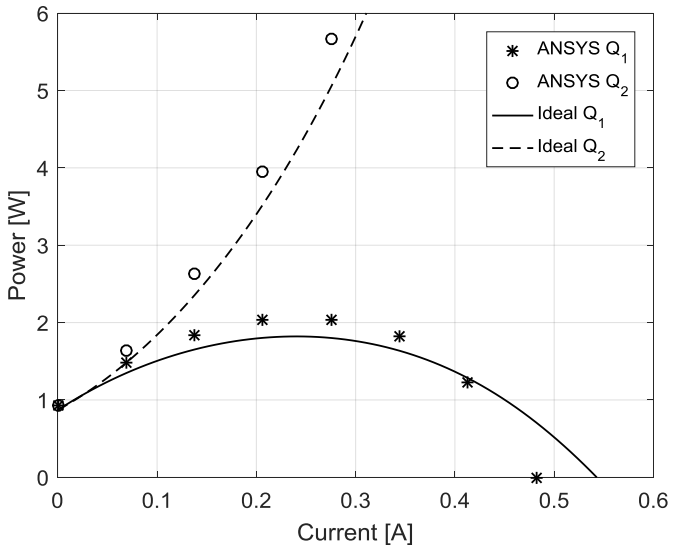

Figure 4. 24 Cooling performance as a function of current.

The use of ANSYS to model the performance lend credence to the results obtained using the ideal equations. Therefore, there is confidence in the design and its predicted performance.

4.6) Other Considerations

This section will briefly cover additional considerations to the design of the self-powered thermoelectric car seat cooler. The two main points here are battery charging and vehicle orientation.

The analysis up to this point assumes that all power generated by the TEG is available for use by the TEC. In practice, this is not always the case. Consideration must be made for the type of charging circuit used. This problem is studied by Kinsella et al. who looked at the various methods to deliver maximum power to a battery connected to a TEG [39]. From their study, it was found that for a temperature difference across the TEG less than $100°C$ a single ended primary inductor converter (SEPIC) is needed to obtain the maximum power. However, this method introduces inefficiencies. From their experiments, an efficiency of 85% is reported.

If a SEPIC is used to charge the battery for the self-powered thermoelectric car seat cooler, then the available power is reduced to $850\ J$. Given this power, the cooler operating at standard conditions and a power draw of $2.39\ W$ can operate for 5.9 minutes. This value is still within the acceptable time frame to allow the cooler to reach steady state.

The other consideration for this device is the orientation of the vehicle during the day. Depending on the specific latitude and longitude and the time of year, the optimal position of the car to receive the maximum solar exposure will vary. It would be cumbersome to require the driver of the vehicle to park in such a way as to align with the sun. However, several studies suggest that the device should receive ample solar exposure in most situations, assuming the device is on one of the front row seats. As previously mentioned, Dadour et al. looked at the temperature variations in a parked car [11]. As part of this study, the solar input through each of the windows was modeled as

the vehicle orientation changed. It is shown that for Crawley, Australia (the location of the study), the front windshield receives the maximum solar exposure if the car is facing north. Conversely, the front windshield receives the least amount of exposure when facing south. When the car is facing either west or east, the solar exposure time is reduced due to the orientation of the sun moving.

Taking this into consideration, the performance of the self-powered thermoelectric car seat cooler is re-evaluated with reduced solar input. The revised solar input for the worst case scenario of the vehicle facing away from the sun is presented in Figure 4. 25. For this case, the maximum solar irradiance is reduced to 500 W/m^2. The resulting generator output is given in Figure 4. 26. Given this performance, the output power is 227 J, which includes the efficiency of the attached SEPIC.

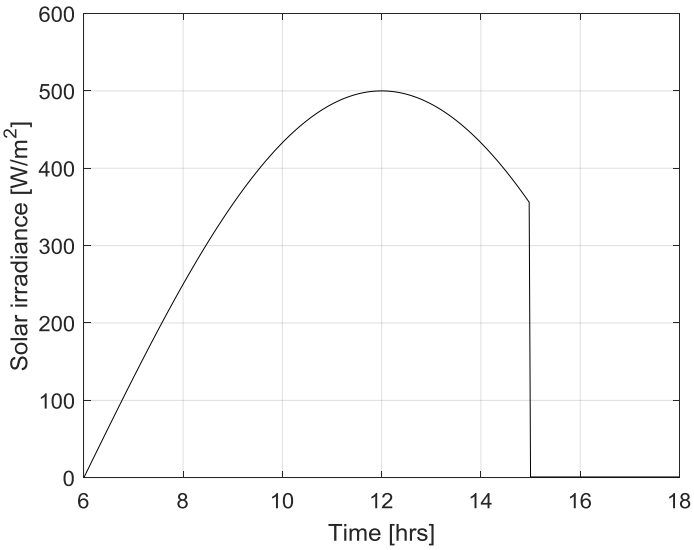

Figure 4. 25 Solar model for the car facing away from sun.

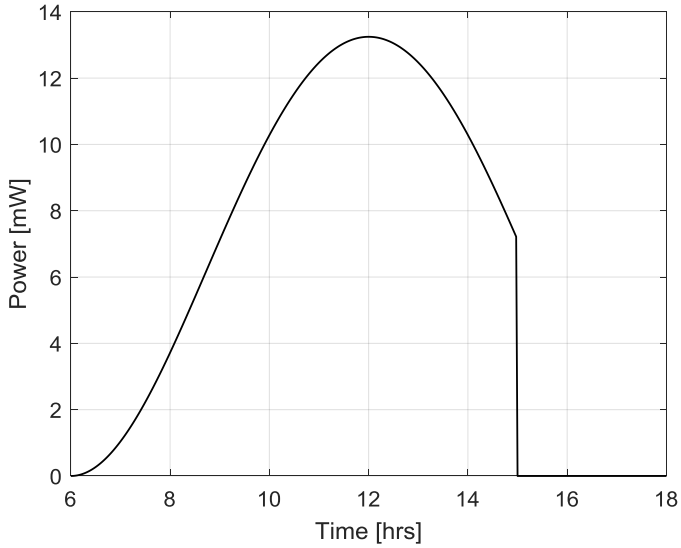

Figure 4. 26 Power output of the generator for the car facing away from the sun.

Given this power output, the seat cooler can operate for 1.6 minutes under average cooling conditions. This amount of time may allow the seat cooler to reach steady state, but will not allow for it to stay there long. A possible solution for this is to provide additional battery storage. This is expanded upon more in the next paragraph.

The last consideration in vehicle orientation is parking locations which allow for no solar exposure. Potentials locations which match this description include under trees, parking garages, home garages, and outdoor coverings. In this situation, the self-powered thermoelectric car seat cooler would not be able to generate any power due to no exposure to the sun. To prepare for situations such as this, the storage capacity should be such that it can hold multiple days' worth of energy. This way, if the car is left in an ideal location for power generation for several days, it can store additional energy to compensate for days which it does not receive any solar energy.

Chapter 5: Conclusions and Future Work

5.1) Conclusions

In this study, the operation of a self-powered thermoelectric car seat cooler is shown to be plausible. Also, it is seen that a single thermoelectric device can be optimized for both power generation and for cooling. This is accomplished by presenting a high level design of the self-powered thermoelectric car seat cooler which displays the system layout and the relationship between the major components. Based on this design, a 1D analytical model is presented which simulates the performance of the device. This model is validated using experimental data. Through a non-dimensional technique, the design is optimized using an iterative process. At the end of the optimization, the ideal parameters are found for the geometric sizing of the thermoelectric, heat sink design, generator load resistance, and the cooler operating current. From this, the size of the absorber plate is chosen.

The ideal parameters fully describe the device. The area of the absorber plate which achieves a temperature difference of $25°C$ under average loading is $0.006\ m^2$. The dimensionless thermal conductance, N_k, is found to be 4.6. This value is a compromise between ideal cooling and power generation. The optimal load resistance ratio, R_r, is 1.7 and the optimal dimensionless current, N_I, for average cooling conditions is 0.375. The optimal value for the non-dimensional convection of the heat sink, N_{2c}, is found to be 11.095.

For the given non-dimensional terms, the designer is free to choose the specific parameters of the device. As long as these chosen parameters still equate to the non-dimensional terms stated, the performance of the device will be identical. The only term

which affects performance is the number of thermoelectric leg pairs. Increasing this term increases voltage and decreases current but, it does not change the power generated.

The design presented is able to generate 1000 J of energy over the course of the simulated day with a maximum power output of 49 mW. The maximum system efficiency is 1% while the maximum thermoelectric efficiency is 2.4%. In cooling operation, the device is able to reduce the seat temperature $25°C$ from the initial temperature while under average loading conditions operating at 0.24 A. The power draw at these conditions is 2.39 W, which allows the seat to operate for about 7 minutes given a full day's worth of energy from the generator. If the cooler is operated at a later time, such as 5:00 PM, when the solar irradiance is less, the device is able to reduce the temperature by $21°C$ at a power draw of 2.3 W.

5.2) Future Work

Going forward from this study, there are several actions which could be taken to make the design more attractive and to test the operation. First, a prototype of this specific design could be built and tested to further validate the performance. This would allow for the study of the device operation under a wide range of operating conditions.

Another application of self-powered thermoelectric car seat cooler is it to use the device as a seat heater in the winter months. The operation would be identical to the cooler, except instead of cooling the absorber plate, the thermoelectric would heat the plate. One main consideration would be the temperature variation of the absorber plate throughout the day during winter months and the total power generated. Proving that the thermoelectric could be used all year round will increase the appeal and usefulness of this device.

References

[1] T.J. Seebeck, 1822, *Magnetic Polarization of Metals and Minerals*, Abhandlungen der Königlichen Akademie der Wissenschaften zu Berlin ed, Berlin, Germany.

[2] Peltier, J. C., 1834, "New Experiments on the Calorific Electric Currents," Ann. Chim. Phys., **56**(2), pp. 371–386.

[3] Thomson, W., 1854, "Account of Researches in Thermo-Electricity," Proc. R. Soc. Lond., **7**, pp. 49–58.

[4] Garvey, L. S., 1979, *Performance Testing of Thermoelectric Generators Including Voyager and LES 8/9 Flight Results*.

[5] "Going 'off the Grid' with BioLite's BaseCamp Stove," Engadget [Online]. Available: https://www.engadget.com/2015/06/24/biolite-basecamp-stove/. [Accessed: 26-Mar-2018].

[6] Baranowski, L. L., Snyder, G. J., and Toberer, E. S., 2012, "Concentrated Solar Thermoelectric Generators," Energy Environ. Sci., **5**(10), pp. 9055–9067.

[7] Bahk, J.-H., Fang, H., Yazawa, K., and Shakouri, A., 2015, "Flexible Thermoelectric Materials and Device Optimization for Wearable Energy Harvesting," J Mater Chem C, **3**(40), pp. 10362–10374.

[8] "II-VI Marlow" [Online]. Available: https://www.marlow.com/industries/automotive. [Accessed: 26-Mar-2018].

[9] 2017, "Gentherm," Gentherm [Online]. Available: http://www.gentherm.com/automotive. [Accessed: 26-Mar-2018].

[10] Zhu, L., Tan, H., and Yu, J., 2013, “Analysis on Optimal Heat Exchanger Size of Thermoelectric Cooler for Electronic Cooling Applications,” Energy Convers. Manag., **76**, pp. 685–690.

[11] Dadour, I. R., Almanjahie, I., Fowkes, N. D., Keady, G., and Vijayan, K., 2011, “Temperature Variations in a Parked Vehicle,” Forensic Sci. Int., **207**(1), pp. 205–211.

[12] Zhang, W., and Liu, J., 2016, “Investigation on the Temporal Surface Thermal Conditions for Thermal Comfort Researches Inside A Vehicle Cabin Under Summer Season Climate,” *MATEC Web of Conferences; Les Ulis*, EDP Sciences, Les Ulis, France, Les Ulis.

[13] Malvicino, C., Mola, S., Zussino, A., and Wolowicz, J., 2001, “The Seat Thermal-Hygrometric Performance Measurement and Its Correlation With Perceived Comfort.”

[14] Bevilacqua, O. M., 1999, “Effect of Air Conditioning on Regulated Emissions for In-Use Vehicles,” Clean Air Veh. Technol. Cent. Oakl. CA Phase Final Rep. Prep. Coord. Res. Counc. Inc Atlanta GA CRC Proj. E-37.

[15] Lee, H., ed., 2016, “Introduction,” *Thermoelectrics: Design and Materials*, John Wiley & Sons, Ltd, pp. 1–7.

[16] Lee, H., ed., 2016, “Applications,” *Thermoelectrics: Design and Materials*, John Wiley & Sons, Ltd, pp. 120–163.

[17] Goldsmid, H. J., Giutronich, J. E., and Kaila, M. M., 1980, “Solar Thermoelectric Generation Using Bismuth Telluride Alloys,” Sol. Energy, **24**(5), pp. 435–440.

[18] Amatya, R., and Ram, R. J., 2010, "Solar Thermoelectric Generator for Micropower Applications," J. Electron. Mater., **39**(9), pp. 1735–1740.

[19] Vinoth, M., and Prema, D., 2014, "Automated Car Safety Seat Cooling System Using Thermoelectric Cooler," *2014 International Conference on Computation of Power, Energy, Information and Communication (ICCPEIC)*, pp. 488–493.

[20] Elarusi, A., 2016, "Optimal Design of a Thermoelectric Cooling/Heating System for Car Seat Climate Control (CSCC)," J. Electron. Mater., **46**(4), pp. 1984–1995.

[21] Feher, S., 1993, "Thermoelectric Air Conditioned Variable Temperature Seat (VTS) and Effect Upon Vehicle Occupant Comfort, Vehicle Energy Efficiency, and Vehicle Environmental Compatibility."

[22] Su, C., Dong, W., Deng, Y., Wang, Y., and Liu, X., 2017, "Numerical and Experimental Investigation on the Performance of a Thermoelectric Cooling Automotive Seat," J. Electron. Mater.

[23] Khattab, N. M., and El Shenawy, E. T., 2006, "Optimal Operation of Thermoelectric Cooler Driven by Solar Thermoelectric Generator," Energy Convers. Manag., **47**(4), pp. 407–426.

[24] Chen, W.-H., Wang, C.-C., and Hung, C.-I., 2014, "Geometric Effect on Cooling Power and Performance of an Integrated Thermoelectric Generation-Cooling System," Energy Convers. Manag., **87**(Supplement C), pp. 566–575.

[25] Du, H., Wang, Y. P., Yuan, X. H., Deng, Y. D., and Su, C. Q., 2016, "Experimental Investigation of a Temperature-Controlled Car Seat Powered by an Exhaust Thermoelectric Generator," J. Electron. Mater., **45**(3), pp. 1529–1539.

[26] Landau, L. D., Bell, J. S., Kearsley, M. J., Pitaevskii, L. P., Lifshitz, E. M., and Sykes, J. B., 2013, *Electrodynamics of Continuous Media*, Elsevier.

[27] Yan, X., Poudel, B., Ma, Y., Liu, W. S., Joshi, G., Wang, H., Lan, Y., Wang, D., Chen, G., and Ren, Z. F., 2010, "Experimental Studies on Anisotropic Thermoelectric Properties and Structures of N-Type Bi2Te2.7Se0.3," Nano Lett., **10**(9), pp. 3373–3378.

[28] Poudel, B., Hao, Q., Ma, Y., Lan, Y., Minnich, A., Yu, B., Yan, X., Wang, D., Muto, A., Vashaee, D., Chen, X., Liu, J., Dresselhaus, M. S., Chen, G., and Ren, Z., 2008, "High-Thermoelectric Performance of Nanostructured Bismuth Antimony Telluride Bulk Alloys," Science, **320**(5876), pp. 634–638.

[29] Kanimba, E., Pearson, M., Sharp, J., Stokes, D., Priya, S., and Tian, Z., 2018, "A Comprehensive Model of a Lead Telluride Thermoelectric Generator," Energy, **142**, pp. 813–821.

[30] Lee, H., 2013, "The Thomson Effect and the Ideal Equation on Thermoelectric Coolers," Energy, **56**, pp. 61–69.

[31] Dias, P. C., Morais, F. J. O., de Morais Franca, M. B., Ferreira, E. C., Cabot, A., and Siqueira Dias, J. A., 2015, "Autonomous Multisensor System Powered by a Solar Thermoelectric Energy Harvester With Ultralow-Power Management Circuit," IEEE Trans. Instrum. Meas., **64**(11), pp. 2918–2925.

[32] "Thermoelectric Generator - EVERREDtronics" [Online]. Available: http://www.everredtronics.com/thermoelectric.generator.html. [Accessed: 05-Apr-2018].

[33] Bar-Cohen, A., and Rohsenow, W. M., 1984, “Thermally Optimum Spacing of Vertical, Natural Convection Cooled, Parallel Plates,” J. Heat Transf., **106**(1), pp. 116–123.

[34] A. Andreas, and T. Stoffel, 1985, *Elizabeth City NREL Report*, DA-5500-56517, Elizabeth City State University, Elizabeth City, North Carolina.

[35] Grundstein, A., Meentemeyer, V., and Dowd, J., 2009, “Maximum Vehicle Cabin Temperatures under Different Meteorological Conditions,” Int. J. Biometeorol., **53**(3), pp. 255–261.

[36] Incropera, F. P., ed., 2011, *Fundamentals of Heat and Mass Transfer*, John Wiley, Hoboken, NJ.

[37] Lloyd, J. R., and Moran, W. R., 1974, “Natural Convection Adjacent to Horizontal Surface of Various Planforms,” J. Heat Transf., **96**(4), pp. 443–447.

[38] Cheng, C.-H., Huang, S.-Y., and Cheng, T.-C., 2010, “A Three-Dimensional Theoretical Model for Predicting Transient Thermal Behavior of Thermoelectric Coolers,” Int. J. Heat Mass Transf., **53**(9), pp. 2001–2011.

[39] Kinsella, C. E., O’Shaughnessy, S. M., Deasy, M. J., Duffy, M., and Robinson, A. J., 2014, “Battery Charging Considerations in Small Scale Electricity Generation from a Thermoelectric Module,” Appl. Energy, **114**(Supplement C), pp. 80–90.